Experimental M1 response of ^{40}Ar as a benchmark for neutrino-nucleus scattering calculations

U. Gayer, T. Beck, M. Bhike, J. Isaak, N. Pietralla, P. C. Ries, D. Savran, M. Schilling, W. Tornow, and V. Werner

Phys. Rev. C **100**, 034305 — Published 9 September 2019

DOI: 10.1103/PhysRevC.100.034305

Experimental $M1$ response of ^{40}Ar as a benchmark for neutrino-nucleus scattering calculations

U. Gayer,[1,*] T. Beck,[1] M. Bhike,[2] J. Isaak,[1] N. Pietralla,[1]
P.C. Ries,[1] D. Savran,[3] M. Schilling,[1] W. Tornow,[2] and V. Werner[1]

[1] *Institut für Kernphysik, Technische Universität Darmstadt, Schlossgartenstraße 9, 64289 Darmstadt, Germany*
[2] *Department of Physics, Duke University and Triangle Universities Nuclear Laboratory, Durham, NC 27708-0308, USA*
[3] *GSI Helmholtzzentrum für Schwerionenforschung GmbH, Planckstraße 1, 64291 Darmstadt, Germany*

(Dated: August 19, 2019)

The excitation of atomic nuclei via magnetic dipole transitions is closely related to the inelastic neutral-current neutrino-nucleus (NC-νA) scattering process due to the similarity of the transition operators. NC-νA-scattering serves for the detection of supernova neutrinos and poses a significant source of background in modern liquid-argon based high-energy neutrino detection experiments. In order to enable tests of the reliability of predictions for neutrino-nucleus scattering, the magnetic dipole response of ^{40}Ar below 7.7 MeV was characterized in a nuclear resonance fluorescence experiment using quasi-monoenergetic gamma-ray beams. The linear polarization of the beams allowed for assignments of electric or magnetic character to previously known dipole excitations. A total magnetic dipole strength of $0.36^{+0.04}_{-0.05}\,\mu_N^2$ was identified in the energy range of the present experiment. Combined with data from previous measurements, the full magnetic dipole strength of ^{40}Ar below the neutron separation threshold was investigated. Due to the low background in the energy range within the bandwidth of the gamma-ray beams, the previous sensitivity limit was improved. A large-scale nuclear shell model calculation in the *sd-fp* space satisfactorily agrees with the data in terms of excitation energies and strengths of the observed 1^+ states.

CONTENTS

I. Introduction 1
A. Motivation 1
B. Current State of Nuclear Structure Studies 2
II. Experiment 3
III. Analysis 3
A. Definitions 3
B. Identification of Transitions 6
1. Newly Observed States 6
2. Unobserved Previously Reported States 6
C. Assignment of J and π Quantum Numbers 7
1. The state at 5392 keV 8
D. Summary 9
IV. Discussion 9
A. Comparison to Shell Model 9
B. Unobserved Branching Transitions 11
1. Direct Decays to the 2_1^+ State 12
2. Observed Population of the 2_1^+ State 12
3. Phenomenological Strength Function 14
C. Unobserved Ground-State Transitions 16
V. Summary 16
Acknowledgments 16
References 17

* ugayer@ikp.tu-darmstadt.de

I. INTRODUCTION

A. Motivation

As a scintillation detector material for weak processes, liquid argon has several advantages over other materials due to its chemical and physical properties, for example its noble-gas character and comparably high density. Consequently, the use of liquid-argon time-projection chambers (LAr-TPCs) for neutrino detection was proposed as early as 1977 by Carlo Rubbia [1]. Today, most accelerator-based neutrino experiments in the world are using LAr-TPCs, like IKARUS [2], ArgoNeuT [3], MicroBooNE [4] and ProtoDUNE [5]. The latter two are prototypes for the Deep Underground Neutrino Experiment (DUNE) [6]. In its final version, DUNE's 'near' LAr-TPC and the two massive 'far' LAr-TPCs will be used to detect neutrinos sent from the Long-Baseline Neutrino Facility (LBNF) at Fermilab to the Sanford Underground Research Facility (SURF). The neutrino beam generated at LBNF consists mainly of high-energy muon-type neutrinos which will be detected via charged-current (CC) reactions on nucleons:

$$\overset{(-)}{\nu}_l + \mathrm{N} \rightarrow l^{\overset{(+)}{-}} + \mathrm{N}'. \tag{1}$$

In this reaction, the absorption of a neutrino of a lepton generation l changes a nucleon N (a proton or a neutron) into its counterpart N′ plus a positively (l^+) or negatively (l^-) charged lepton of generation l. In addition, the two aforementioned LAr-TPCs will also become the most powerful detectors for neutrinos from core-collapse supernova explosions. The associated neutrino energy

spectrum is centered at approximately 10 MeV [7]. Here, CC interactions allow for the detection of electron-type neutrinos, predominantly via the two reactions

$$\nu_e + \mathrm{Ar} \rightarrow \mathrm{K}^* + e^- \tag{2}$$

$$\bar{\nu_e} + \mathrm{Ar} \rightarrow \mathrm{Cl}^* + e^+, \tag{3}$$

while the neutral-current (NC) interaction

$$\nu + \mathrm{Ar} \rightarrow \nu' + \mathrm{Ar}^* \tag{4}$$

is ideal for detecting all neutrino flavors via magnetic dipole excitations of the most abundant argon isotope ^{40}Ar. Of course, the high-energy neutrino beam from LBNF will also generate NC nuclear excitations of ^{40}Ar and will undergo CC absorption on ^{40}Ar nuclei as well.

Count-rates and background contributions in neutrino experiments are usually estimated using Monte-Carlo event generators like GENIE [8] or GEANT4 [9–11]. Because neutrinos from earth-based and cosmic sources cover energy scales from about 0.1 MeV up to the EeV [12] regime, these codes employ piece-wise constructed models for neutrino-matter interactions with different levels of model dependence and phenomenology. In the following, the discussion is restricted to low-energy neutrinos of a few MeV. This energy range is not only of special interest for supernova neutrinos, but also for neutrino experiments in general, because it corresponds to the dominant part of the spectrum of the most intense source of neutrino background, the sun. However, the theoretical description of the neutrino-nucleus interaction is challenging due to the significant influence of nuclear structure effects [13]. Unfortunately, experimental data are scarce and direct neutrino-nucleus scattering data exist only for a handful of nuclei, because the experiments are time-consuming and challenging. Most notably, cross sections for various reaction channels at different energies have been measured for ^{12}C by the E225 [14], KARMEN [15] and LSND [16] collaborations. If possible, one usually resorts to the study of inverse or analog reactions, where the structure of the transition operator is similar to neutrino processes. The following subsection summarizes the existing experimental and theoretical studies of the nucleus ^{40}Ar related to neutrino scattering.

B. Current State of Nuclear Structure Studies

The case of LAr is, on the one hand, advantageous for nuclear physics studies, because the isotope ^{40}Ar has a very high natural abundance of 99.6035(25) % [17] which makes the element practically monoisotopic. On the other hand, the neutron excess, shell structure and deformation of this isotope make it a challenge for theoretical nuclear models. Due to the popularity of LAr-TPCs, many theoretical predictions of the ^{40}Ar neutrino-nucleus cross section have been published in the last years, tackling the neutrino-nucleus problem with the plane-wave impulse approximation [18], quasiparticle random phase approximation (RPA) [19], relativistic quasiparticle RPA [20], relativistic distorted-wave impulse approximation [21], transport theory [22] and continuum RPA [23]. On the experimental side, ^{40}Ar has been studied in low-energy elastic [24] and high-energy inclusive inelastic [25] electron scattering experiments, the latter of which was used to test theoretical weak form factors [21]. Furthermore, the Gamow-Teller strength [B(GT)] distribution for the transition from ^{40}Ar to excited states of ^{40}K was estimated from the beta-decay of its isospin-symmetry partner ^{40}Ti [26] and measured directly using the (p,n) charge-exchange reaction on ^{40}K [27]. This is the dominant part of the CC contribution to the neutrino-matter cross section at low energies. Theoretical studies [19] and the ^{12}C data indicate that the so far unconstrained NC part, given by Eq. (4), contributes roughly 10 % to the total neutrino-nucleus cross section. It is well known, see e.g. Ref. [28], that the NC transition operator, the zero-component of the Gamow-Teller operator

$$\mathbf{O}(\mathrm{GT}_0) = \sum_k 2\mathbf{s}(k)\mathbf{t}_0(k), \tag{5}$$

has a similar structure as the spin part of the isovector magnetic dipole ($M1$) operator. The complete isovector $M1$ operator, including the orbital part, has the following form:

$$\begin{aligned}\mathbf{O}(M1)_{\mathrm{iv}} = \sqrt{\frac{3}{4\pi}} \sum_k & (g_l^p - g_l^n)\mathbf{l}(k)\mathbf{t}_0(k) \\ & + (g_s^p - g_s^n)\mathbf{s}(k)\mathbf{t}_0(k).\end{aligned} \tag{6}$$

In Eqs. (5) and (6), the sum runs over all nucleons k, and $\mathbf{s}(k)$ and $\mathbf{t}(k)$ are the spin and isospin operators for single nucleons, respectively. The single-particle orbital angular momentum operator is denoted as $\mathbf{l}(k)$. The symbols g denote the orbital (l) and spin (s) g-factors for protons (p) and neutrons (n), which can have effective values in a truncated model space that deviate from their bare values. Using the similarity between $\mathbf{O}(\mathrm{GT}_0)$ and $\mathbf{O}(M1)_{\mathrm{iv}}$, experimental data on the $M1$ response can therefore be used to constrain models of the NC neutrino scattering cross sections. In contrast to Ref. [28], the large deformation of ^{40}Ar ($\beta = 0.266(6)$ [29]) does not allow to fully neglect the orbital $M1$ strength in the energy range of the present experiment, because spin-$M1$ strength is expected to be in competition with low-lying orbital $M1$ strength of the so-called scissors mode [30]. In addition to measurements of the total $M1$ strength, spectroscopy is needed to constrain the distribution of $M1$ strength, which manifests itself as well-separated quantum states at the energies of interest.

Based on the aforementioned similarity of Gamow-Teller and $M1$ operators, we chose to study the $M1$ response of ^{40}Ar below the neutron separation threshold using the nuclear resonance fluorescence (NRF) technique

[31] after excitation with a quasi-monoenergetic, almost completely linearly polarized photon beam [32]. This experimental method allows to selectively study dipole-excited states with a high degree of model-independence. However there is no sensitivity to the aforementioned orbital- and spin contributions to an $M1$ excitation [33]. For the separation of both parts, theoretical models have to be employed as, for example, in [28] and [34]. First results in the energy range from 7.7 to 11 MeV have already been published [35]. The single $M1$ excitation observed by Li *et al.* [35] was described well by a calculation in the nuclear shell model (SM) in the *sd-fp* configuration space using Nowacki's interaction [36], which predicts a larger part of the $M1$ strength to be located at even lower excitation energies. This energy region was covered in the present experiment.

This article is structured as follows: The experimental setup and procedure will be described in section II. Section III defines relevant quantities, explains the analysis of the raw data in detail and presents the data. A discussion of the results, with a focus on the estimation of the unobserved B($M1$) strength, can be found in section IV, which is followed by a summary in section V.

II. EXPERIMENT

The experiment utilized the quasi-monochromatic, almost completely linearly polarized photon beam of the High-Intensity γ-ray Source (HIγS) [37]. In a previous experiment, which used unpolarized bremsstrahlung as a photon source, Moreh *et al.* [38] determined excitation energies, integrated cross sections and angular momentum quantum numbers J of dipole- and quadrupole-excited states of ^{40}Ar in the energy range up to 11 MeV. Based on these data, the photon beam of HIγS was tuned to centroid energies of 4.44(19), 5.40(19), 5.65(21), 5.90(24), 6.10(24), 6.30(24), 6.50(26), 6.70(26), 6.90(28), 7.22(31), and 7.55(33) MeV. With the full width at half maximum (FWHM) of the approximately Gaussian beam profile given in parentheses after the centroid energies[1], the energy range from about 4.2 MeV to about 7.7 MeV was scanned. The range between the first and the second energy setting was skipped, because only one strongly excited state is located there, whose parity π was already found to be negative in an NRF experiment with polarized bremsstrahlung [39]. At each energy setting, data were taken for about 1-3 h. The target was a high-pressure gas container filled with natural argon gas at 4500 PSI, in the same arrangement as in Ref. [35]. Photons scattered off the target were detected by four HPGe detectors with detection efficiencies of 60 % compared to a standard NaI detector at 1.33 MeV at polar angles of $\theta = 90°$ with respect to the beam axis and at azimuthal angles of $\varphi = 0°$, 90°, 180° and 270°, where $\varphi = 0°$ and $\varphi = 180°$ define the polarization axis. All detectors were mounted at a distance of 90(2) mm to the beam axis around the ^{40}Ar target. A schematic drawing of the setup is shown in Ref. [35], where the same geometry was used. The symbols $\parallel$ and $\perp$ will be used in the following to denote detectors mounted in the beam's polarization plane or perpendicular to it. In order to identify contaminant transitions from constituents of the gas container and the shielding, measurements with an identical empty container were done at intermediate energies of 5.65, 5.90, 6.10, 6.50, 6.90 and 7.22 MeV for approximately the same measuring time as used for the argon gas.

Experimental spectra at a beam energy of 7.22(FWHM: 0.31) MeV are shown in FIG. 1. Since the orientations of both detectors parallel or perpendicular to the beam's polarization plane are equivalent in the present experiment, the measured spectra have been rebinned and summed to show the total acquired statistics. From the background (BG) transition of an unknown nuclide at 7212 keV, it can be seen that the time-integrated photon flux was similar in the measurement with the empty container and with the argon container. This transition was used to normalize the spectra of the empty container and the argon runs to each other to be able to subtract the background contribution from the transition at 7246 keV. A similar reference transition was found in all other cases where a transition from ^{40}Ar overlapped with background.

In the following section, the relevant formalism for the extraction of the observables from the raw spectra will be introduced, and the results will be presented.

III. ANALYSIS

This section consists of four subsections. In subsection III A, the relevant quantities for the analysis and the following section IV are defined. Subsection III B discusses the identification of transitions and the assignment to excited states. The following subsection III C describes how angular momentum and parity quantum numbers were assigned. It is followed by a short summary (subsection III D).

A. Definitions

The number of detected events $A_{i\to f}$ for an isolated transition from a state i, which was resonantly excited by the beam from the ground state '0' to a final state f,

[1] In the following, occurrences of beam energies in the text will include an 'FWHM' label to distinguish the notation from the usually quoted 1σ interval.

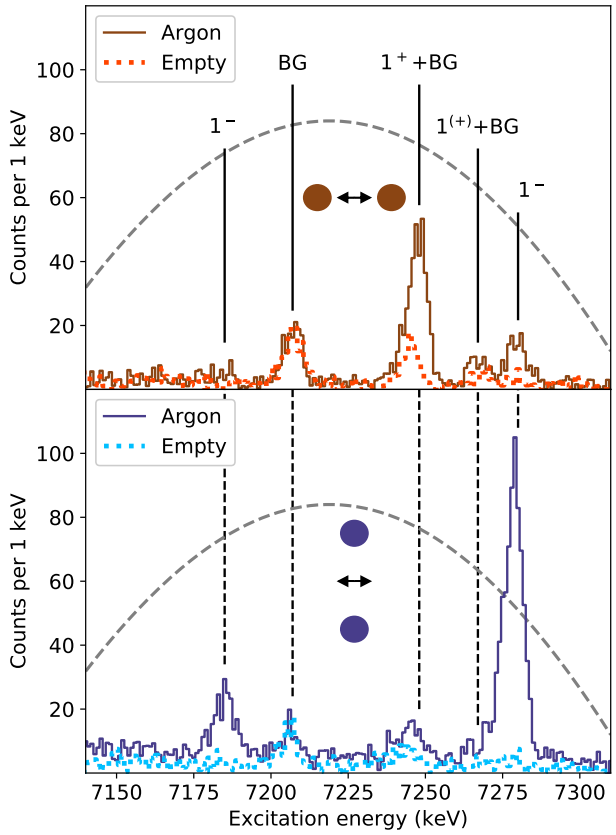

FIG. 1. Experimental spectra of the empty and the filled gas container, at a beam energy of 7.22(FWHM: 0.31) MeV. The beam intensity distribution in arbitrary units is indicated by a grey dashed line in both panels. In the upper (lower) panel, the spectra of the detectors inside (outside) the beam polarization plane are shown. The inset graphics indicate the polarization plane (double-sided arrow) and the location of the detectors (filled dots). The assignment of observed transitions, either to ^{40}Ar (J^π) or background (BG) is indicated at the respective energies.

is given by

$$A_{i\to f} = N_\mathrm{T} N_\gamma(E_i) I_{0\to i\to f} \times \int_\Omega \epsilon(E_i - E_f, \Omega) \frac{W_{0\to i\to f}(\Omega=\theta,\varphi)}{4\pi} \mathrm{d}\Omega. \quad (7)$$

In Eq. (7), E_i and E_f denote the excitation energies of states with the labels i and f, N_T is the number of target nuclei, $N_\gamma(E)$ is the time-integrated number of photons per area and energy interval, $I_{0\to i\to f}$ is the energy-integrated cross section of the absorption and emission sequence that leads to the observed transition, ϵ is the photopeak-efficiency of the setup, and $W_{0\to i\to f}$ is the angular distribution function of the decay transition [40] which depends on the states' angular momentum (J) and parity (π) quantum numbers. The integration of the product of the efficiency and the angular distribution over the solid angle Ω implies that the finite extent of the detectors and the relatively large target have to be taken into account. In practice, this was done using a GEANT4 [9–11] simulation of the setup. The simulated energy dependence of the efficiency was validated by comparison to an off-beam measurement with a point-like radioactive ^{56}Co [41] source at the target position[2]. For the discussion of the results of an NRF experiment, note that $I_{0\to i\to f}$ is given by [33]:

$$I_{0\to i\to f} = \pi^2 \left(\frac{\hbar c}{E_i}\right)^2 \underbrace{\frac{2J_i+1}{2J_0+1}}_{g} \Gamma_{0\to i} \frac{\Gamma_{i\to f}}{\Gamma_i}. \quad (8)$$

In Eq. (8), J_0 and J_i denote the angular momentum quantum numbers of the ground state and the excited state, respectively. They are included in the statistical factor g which takes into account that the transition can occur between different degenerate magnetic substates. The sequence of resonant absorption followed by a direct transition to the ground state will be denoted as 'elastic' photon scattering in the following, in analogy to actual scattering experiments. The symbol

$$\Gamma_i = \sum_f \Gamma_{i\to f} = \sum_f \sum_{\{\lambda L\}} \Gamma_{i\to f,\lambda L} \quad (9)$$

denotes the total transition width of the excited state, which is the sum of partial transition widths $\Gamma_{i\to f}$ for all possible decay channels. Above the neutron separation threshold, 'all possible decay channels' also include decays via particle emission, but in this experiment, the excitation energies are sufficiently low, so that only gamma-decay channels are included in Γ_i in Eq. (9). A single partial transition width $\Gamma_{i\to f}$, as indicated in the second part of Eq. (9), is a sum of contributions of all allowed electromagnetic characters λ ('E' for electric or 'M' for magnetic) and multipole orders L. In the following, the branching ratio will be defined as the ratio of a single transition width to the total transition width:

$$\frac{\Gamma_{i\to f}}{\Gamma_i} = \frac{\Gamma_{i\to f}}{\sum_g \Gamma_{i\to g}} = \frac{I_{0\to i\to f}}{\sum_g I_{0\to i\to g}}. \quad (10)$$

The last equality follows from Eq. (8). In experiments with quasi-monochromatic photon beams, a so-called 'average branching ratio' [42–49] of photoexcited states is often accessible, if discrete states cannot be resolved any

[2] Note that in all actual calculations, relative efficiencies instead of the absolute efficiencies that appear in Eq. (7)were used, since they are independent of the uncertainty of the source activity.

more. It is defined as:

$$\begin{aligned}\langle b_f\left(E_{\mathrm{beam}};J^\pi\right)\rangle &\equiv \frac{\sum_i I_{0\to i\to f}}{\sum_i\sum_g I_{0\to i\to g}}\\ &\overset{\text{Eq. (8), (9)}}{=} \frac{\sum_i \Gamma_{0\to i}{}^{\Gamma_{i\to f}/\Gamma_i}}{\sum_i \Gamma_{0\to i}}\\ &= \frac{\langle\Gamma_{0\to i}{}^{\Gamma_{i\to f}/\Gamma_i}\rangle}{\langle\Gamma_{0\to i}\rangle} \neq \left\langle\frac{\Gamma_{i\to f}}{\Gamma_i}\right\rangle,\end{aligned} \tag{11}$$

Compared to Eq. (10), both the numerator and the denominator of Eq. (11) contain a sum over the label i, which is assumed to be a sum over all states with quantum numbers J^π populated directly by the beam. If there is no sensitivity to the quantum numbers of the excited states, the labels J^π will be dropped. The notation $\langle\ldots\rangle$ indicates the average value of a quantity. Note that the ratio of the (in-)elastic and the total cross section in Eq. (11), which can be obtained from experimental data in a straightforward way (see also the following discussion about Eq. (12)), is not exactly equal to the literal 'average branching ratio', which is indicated by the last symbol of inequality. Even if all the $\Gamma_{i\to f}$ were statistically independent, as it is often assumed in the statistical model (see, e.g. [50]), the last equality would not be exact, since Γ_i depends on the values of all $\Gamma_{i\to f}$, and therefore $\langle\Gamma_{0\to i}{}^{\Gamma_{i\to f}/\Gamma_i}\rangle \neq \langle\Gamma_{0\to i}\rangle\langle{}^{\Gamma_{i\to f}/\Gamma_i}\rangle$, for example. The quantity $\langle b_f\rangle$ actually represents the average branching ratio weighted by the ground-state transition widths $\Gamma_{0\to i}$. In accordance with the literature, in particular [44, 45, 47], it will still be denoted as 'average branching' in the following.

The value $1-\langle b_0\rangle$ can be interpreted as the average branching ratio to all excited states, and it will be used below to estimate missing strength due to unobserved branchings. In order to obtain this quantity from an NRF experiment, it is evident from Eqs. (10) and (11) that all branching transitions of a state need to be known. In an NRF measurement, this is often not possible and a quoted value of ${}^{\Gamma_{i\to f}}/_{\Gamma_i}$ will be an upper limit for the 'true' branching ratio. To account for unobserved branching transitions to excited states, it is commonly assumed that the decay eventually cascades via the 2_1^+ state in even-even nuclei [42–49]:

$$\begin{aligned}\sum_{f>0} I_{0\to i\to f} \geq\ & I_{0\to i\to 2_1^+\to 0} + \sum_j I_{0\to i\to j\to 2_1^+\to 0}\\ &+ \sum_j\sum_k I_{0\to i\to j\to k\to 2_1^+\to 0} + \ldots\\ \equiv\ & I_{i\Rightarrow 2_1^+}.\end{aligned} \tag{12}$$

On the right-hand side of Eq. (12) is a sum over all possible multistep cascades that can populate the 2_1^+ state (single-, two- and three-step cascades from the state i are shown). The quantity $\sum_i I_{i\Rightarrow 2_1^+}$ can be obtained from the counted events of the $2_1^+\to 0_1^+$ transition in the experiment. Using the aforementioned definitions, an approximation for the average ground-state branching $\langle b_0\rangle$ that uses experimentally accessible quantities only, can be derived:

$$\begin{aligned}\langle b_0\rangle &\overset{\text{Eq. (11)}}{=} \frac{\sum_i I_{0\to i\to 0}}{\sum_i I_{0\to i\to 0} + \sum_i\sum_{f>0} I_{0\to i\to f}}\\ &\overset{\text{Eq. (12)}}{\leq} \frac{\sum_i I_{0\to i\to 0}}{\sum_i I_{0\to i\to 0} + \sum_i I_{i\Rightarrow 2_1^+}}.\end{aligned} \tag{13}$$

The second experimental observable that is used in Eq. (13), $\sum_i I_{0\to i\to 0}$, is the total elastic cross section within the excitation energy range defined by the width of the beam. Note that here the sensitivity limit of the experiment for the detection of ground-state transitions was neglected. In section IV, it will be shown that this is a valid approximation for the present experiment, since the impact of unobserved branching transitions on the total strength is estimated to be about a factor of 10 higher than the unobserved ground-state transitions.

The partial transition widths can be related to the reduced transition strength $B(\lambda L; f\to i)$ of the excitation from the state f to i with electromagnetic character λL [33]:

$$\begin{aligned}\Gamma_{i\to f} = 8\pi \sum_{\{\lambda L\}} &\frac{L+1}{L\left[(2L+1)!!\right]^2}\left(\frac{E_i-E_f}{\hbar c}\right)^{2L+1}\\ &\times\frac{2J_i+1}{2J_f+1}\mathrm{B}(\lambda L; i\to f).\end{aligned} \tag{14}$$

The quantity $\mathrm{B}(\lambda L; i\to f)$ will be abbreviated as $B(\lambda L)\uparrow$ in the following if the involved states are obvious from the context. Note that the reduced transition strength for decay, $B(\lambda L)\downarrow$, differs from the excitation strength due to the presence of the factor ${}^{2J_i+1}/_{2J_f+1}$ in Eq. (14). From Eqs. (8), (9), and (14) it is obvious that the reduced transition strength can only be accessed if the so-called ground-state branching ratio ${}^{\Gamma_{i\to 0}}/_{\Gamma_i}$ is known. Another requirement is that the relative contributions of different multipoles have to be known. They can be quantified by the multipole-mixing ratio in the convention of Krane, Steffen and Wheeler [40]:

$$\begin{aligned}\delta^2 = \frac{\Gamma_{i\to f,\lambda'(L+1)}}{\Gamma_{i\to f,\lambda L}} &= \frac{L(L+2)}{(L+1)^2(2L+3)^2}\\ &\times\left(\frac{E_i-E_f}{\hbar c}\right)^2\frac{\mathrm{B}(\lambda'(L+1))}{\mathrm{B}(\lambda L)}.\end{aligned} \tag{15}$$

For the elastic transitions considered in the present case, only the lowest possible multipole is allowed due to $J_0^{\pi_0}=0^+$ for the ground state of ^{40}Ar.

We report all resolved transitions whose total number of observed events $A_{i\to j}^{\mathrm{tot}}$ in all detectors fulfilled the inequality

$$A_{i\to f}^{\mathrm{tot}} > 2.3\sqrt{A_{i\to f}^{\mathrm{bg}}}, \tag{16}$$

where $A_{i\to f}^{\mathrm{bg}}$ denotes the integrated quasi-continuous background on which the observed transition is located.

The criterium corresponds to a confidence level of 95 % [51].

For the calculation of all derived quantities in this publication, the general Monte-Carlo method suggested in the "Guide to the expression of uncertainty in measurement" (GUM) [52] was applied. This was deemed necessary due to the low statistics of several observed transitions. The input quantities A, ϵ and E_i from Eq. (7), if obtained by the application of least-square fitting algorithms, were assumed to be normal-distributed within the uncertainty estimate given by the algorithm. Similarly, the quantities E_i and I, if derived from literature values, were also assumed to follow a normal distribution. The propagation of uncertainties employed 10^6 randomly sampled values from the input distributions. Asymmetric uncertainties for all derived quantities are quoted. They are obtained from the most probable value and the shortest coverage interval of the distribution of the derived quantity, after the truncation of unphysical values in the sense of Bayesian statistics [52]. The given shortest coverage interval has been chosen to cover 68.27 % of the distribution, i.e. the given uncertainty can be interpreted in a similar way as a 1σ interval for a normal distribution.

In the following subsection, the assignment of several lines in the spectrum to transitions between states of ^{40}Ar is described in detail.

B. Identification of Transitions

The first part of this subsection discusses the determination of the elastic cross section of newly observed states. Since the present experimental method allowed for a straightforward discrimination of ground-state and excited-state transitions, some previously identified excited states were not confirmed. Their updated assignment is discussed in the second part.

1. Newly Observed States

Ground-state transitions of previously unknown states were observed at 5656 , 5850 , 6084 , 6284 , 6566 , 6922 , and 7190 keV, all of which escaped detection in Ref. [38] because of the lower sensitivity of that experiment. Their gamma-ray energy E_γ was determined relative to known transitions of ^{40}Ar [29] or transitions from contaminants (see also Sec. III C and Tab. II). The given level energies E_i have been obtained from the measured E_γ by correcting for the recoil of the ^{40}Ar nucleus during the absorption- and emission process [53]. In order to determine their elastic photon scattering cross sections, the product

$$C_{0\to i\to f}(E_i, E_f) \equiv N_T N_\gamma \int_\Omega \epsilon \frac{W_{0\to i\to f}}{4\pi} \mathrm{d}\Omega = \frac{A_{i\to f}}{I_{0\to i\to f}} \tag{17}$$

in Eq. (7), which is the ratio of the observed events A (the experimental observable) and the integrated cross section I (the quantity of interest), was calibrated as follows: The energy dependence of C was inferred using measurements of the attenuated beam-photon spectrum and the energy-dependent detection efficiency. The absolute scale of Eq. (17) was calibrated using transitions of ^{40}Ar with a known elastic photon scattering cross section observed at the same beam-energy setting. If no such reference transition was available in the same spectrum, the photon flux was calibrated relative to another beam energy setting by comparison of the low-energy regions of the spectra. This procedure is described in Refs. [54–56]. Mostly due to the imprecise knowledge of the structure of the target container, the GEANT4 simulations of the low-energy region deviated by up to 20 % from the experimental spectra. This percentage was used as an estimate of the systematic uncertainty of this procedure. The excitation cross sections of all new states are so low that they could not have been observed by Moreh *et al.* [38].

2. Unobserved Previously Reported States

According to the sensitivity limit given by Eq. (16), excited states at 5912 , 6450 , 6703 and 7168 keV, which were reported by Moreh et al. [38], were not observed despite the higher sensitivity of the current experiment. They were most likely the result of a false assignment, since transitions of higher-lying states to other excited states and ground-state transitions may appear at similar energies in experiments with bremsstrahlung photons. This hypothesis is supported by the fact that all of these previously claimed states were assigned a low excitation cross section, causing low statistics in the data of Ref. [38] and preventing a clear spin assignment using angular correlations. TABLE I gives a list of known excited states of ^{40}Ar with excitation energies E_i and quantum numbers $J_i^{\pi_i}$ from which a gamma ray with one of these four energies could have been emitted in a transition to a known lower-lying excited state. The candidates were determined using the Ritz variation principle [57] with the following boundary condition:

$$|(E_i - E_f) - E_\gamma| \leq \sqrt{\Delta E_i^2 + \Delta E_f^2} + \Delta E_\gamma. \tag{18}$$

Eq. (18) states that E_γ, a gamma-ray energy which could not be assigned to a ground-state transition, should not differ from an energy difference between two other known states by more than the sum of the 1σ intervals. Not all the possible origins of gamma rays in TABLE I are equally probable. Gamma-ray transitions usually favor low multipolarities, therefore a transition between the dipole- or quadrupole-excited state at 9912 keV to the 6^+ state at 3465 keV, or a direct excitation of a 12^+ state, for example, are highly unlikely. Furthermore, for excited states above the neutron separation threshold of ^{40}Ar of 9869 keV [29], gamma decays are in competition with

dominant particle decays. However, these two restictions still leave at least one possible transition between excited states that could account for the false assignment in the previous bremsstrahlung experiment.

Another transition which was not observed is the ground-state decay of the 1^- state of ^{40}Ar at 4481.0(3) keV, reported in the Evaluated Nuclear Structure Data Files (ENSDF) [29] with a given upper limit for the lifetime $\tau_{4481} < 0.07$ ps ($\tau_{4481} < 0.1$ ps in the original publication [58]), which corresponds to a lower limit for the total width of $\Gamma_{4481} > 0.009$ eV ($\Gamma_{4481} > 0.007$ eV [58]). The total width $\Gamma = 0.070(13)$ eV [29] of the observed 1^+ state at 4473(1) keV, which is very close in energy, was used in Eq. (16) and (17) to obtain an upper limit of $\Gamma_{4481} < 0.0041(8)$ eV for the total width of the state at 4481 keV. Note that this estimate was made under the assumption $\Gamma_{4481\to0}/\Gamma_{4481} = 1$ for both states. Therefore, the disagreement of the lower and upper limits could be resolved if other branching transitions exist, since the $(p, p'\gamma)$ experiment of Southon *et al.* [58] measured the lifetime/total width with the Doppler-shift attenuation method (DSAM), while the present NRF experiment is only sensitive to $\Gamma^2_{4481\to0}/\Gamma_{4481}$.

TABLE I. Possible initial (i) and final states (f) for gamma rays that have, with a high probability, been falsely interpreted as ground-state transitions in the experiment of Moreh *et al.* [38]. All potential initial and final states were taken from the Evaluated Nuclear Structure Data Files (ENSDF) [29], which are also the source for all given energies and quantum numbers. Ranges of possible values for J and π are given in the ENSDF format. To match the gamma-ray energy to an energy difference between two states, the criterion in Eq. (18) was used. Since the experiment of Moreh *et al.* [38] had a maximum endpoint energy of 11.8 MeV, only initial states up to this energy were considered. No restriction on the difference in the angular momentum quantum number was imposed here , which means that some of the candidates given below are extremely unlikely and only listed for completeness (see also the discussion in the main text).

E_γ keV	E_i keV	$J_i^{\pi i}$	E_f keV	$J_f^{\pi f}$
5912(3)	8032(3)	(1^-)	2120.91(17)	0^+
	9373(4)		3464.56(12)	6^+
	9425(5)	$(1^-, 2^+)$	3515(1)	4^+
	9433(5)	$(1^-, 2^+)$	3515(1)	4^+
	9596(4)		3680.60(12)	3^-
	9825(3)	1^-	3918.85(12)	2^+
	9851(3)	1^-	3941.9(2)	
	9952(3)	1^-	4042(2)	NATURAL
	10090(3)	1^-	4178.9(3)	
	10857(3)	1^-	4942.6(4)	
6450(3)	9337(3)	1^-	2892.65(9)	4^+
	9656(4)	1^-	3207.93(13)	2^+
	9912(5)	$(1^-, 2^+)$	3464.56(12)	6^+
6703(3)	8163(2)	1^-	1460.849(5)	2^+
	9234(4)	1^-	2524.09(11)	2^+
	9596(4)		2892.65(9)	4^+
	9912(5)	$(1^-, 2^+)$	3207.93(13)	2^+
	10745(3)	1^-	4042(2)	NATURAL
7168(3)	9287(4)		2120.91(17)	0^+
	9296(5)	$(1^-, 2^+)$	2120.91(17)	0^+
	9690(5)	$(1^-, 2^+)$	2524.09(11)	2^+
	11769(?)	(12^+)	4602(1)	

C. Assignment of J and π Quantum Numbers

The goal of this experiment was the identification of magnetic dipole strength. This was accomplished by observation of the angular distribution W of the emitted gamma rays. It depends on the parity and angular momentum quantum numbers of a cascade of transitions when a beam of polarized photons is used for the excitation [31, 32]. Figure 2 shows the asymmetry

$$\varepsilon = \frac{A_\parallel/\epsilon_\parallel - A_\perp/\epsilon_\perp}{A_\parallel/\epsilon_\parallel + A_\perp/\epsilon_\perp} \equiv \frac{N_\parallel - N_\perp}{N_\parallel + N_\perp} \approx \Sigma Q P \qquad (19)$$

of the counted numbers of events for observed ground-state transitions. The numbers of events have been normalized by the efficiencies $\epsilon_\parallel$ and $\epsilon_\perp$ of the detector pairs. In Eq. (19), the asymmetry is related to the analyzing power of azimuthal Compton polarimetry

$$\Sigma = \frac{W(90°, 0°)_{0\to i\to f} - W(90°, 90°)_{0\to i\to f}}{W(90°, 0°)_{0\to i\to f} + W(90°, 90°)_{0\to i\to f}}. \qquad (20)$$

Σ is equal to $+1$ (-1) for $0^+ \to 1^+ \to 0^+$ $(0^+ \to 1^- \to 0^+)$ cascades. The symbol P represents the polarization of the incident beam, which has previously been measured to exceed 99 % [37], and Q denotes the polarization sensitivity of the experimental setup. In the present analysis, Q was simulated using GEANT4 for different cascades and the resulting calculated asymmetries were compared to the experimental data to determine J and π quantum numbers. Photons in the simulation were emitted from all parts of the argon target that are traversed by the beam, i.e. where NRF reactions could take place. Due to the extended target and the finite solid angles of the detectors, Q amounts to about 0.75 . This value is in good agreement with the data, as can be seen in FIG. 2. It is larger than the value of 0.5 determined by a fit to experimental asymmetries in Ref. [35], probably because that experiment utilized a collimator for the gamma-ray beam with a larger diameter (1 inch compared to 0.75 inch in the present experiment). Compared to the experimental uncertainties of the asymmetries, the energy dependence of Q was found to be negligible. The dominantly statistical uncertainty of the asymmetries is sufficiently small for parity assignments in most cases. Explicitly, $J^\pi = 1^+$ $(J^\pi = 1^-)$ was assigned, if the experimental

asymmetry was in unambiguous agreement with a positive (negative) assignment within its 1σ uncertainty shown in FIG. 2. If this was not the case, due to the restriction of parity and angular momentum to integer values, a positive (negative) parity was assigned if more than 95 % of the probability distribution of the experimental value is above (below) $\varepsilon = 0$ (an example is the state at 6084 keV).

A discrimination of dipole- and quadrupole excitations, if not already done by Moreh *et al.* [38] , was more challenging with the given statistics and sensitivity of the setup. If the asymmetry of a ground-state transition was negative, $J^\pi = 1^-$ was assigned, because the competing magnetic quadrupole excitations are suppressed both due to their magnetic character and their higher multipolarity. This is supported by the fact that only little $M2$ strength was observed in ^{36}Ar and ^{38}Ar in an electron scattering experiment by Foltz *et al.* [59]. For newly observed positive parity states, the aforementioned arguments are not applicable and the assignment of dipole character is tentative. In addition, FIG. 2 contains asymmetries of transitions from contaminants, which were distinguished from transitions of ^{40}Ar using the measurements with the empty gas bottle. Angular distributions of de-exciting transitions of nuclei with half-integer spins are generally less asymmetric. Indeed, all transitions with a low asymmetry were found in the known level scheme of ^{27}Al [60]. For some of the observed states of ^{27}Al, there are uncertain J^π assignments in [60], and it has been demonstrated in previous studies, for example [61], that these can be resolved also for odd-even nuclei using the NRF technique with quasi-monochromatic gamma-ray beams. However, the differences in the simulated asymmetry ϵ^{sim} of the possible spin- and parity assignments are small, especially after a correction for the geometry of the large argon target, and they would require statistical uncertainties on the order of a few percent. Furthermore, since the exact composition and the distribution of the aluminium in the gas bottle is unknown, the simulated asymmetries themselves contain a systematical uncertainty. For this reason, it is not possible to make a significant contribution to the ^{27}Al literature data with the present dataset. The other main constituent of the gas bottle, carbon (^{12}C), produces a transition from its first 2^+ state at 4440 keV [62] with an observed asymmetry that is consistent with a 2^+ assignment.

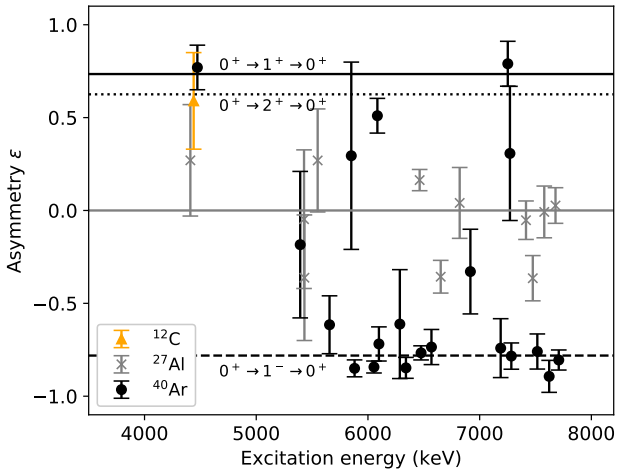

FIG. 2. Experimental count-rate asymmetry of ground-state transitions between the detector pairs parallel and perpendicular to the beam polarization plane. The measured values are compared to simulated asymmmetries for photons emitted from the part of the ^{40}Ar volume which was traversed by the beam, after different spin sequences (solid, dotted and dashed black lines with labels).

1. *The state at* 5392 keV

The criteria defined earlier in this section leave the state at 5392 keV with an uncertain parity assignment. It is, however, very close in energy to a state at 5400.5(8) keV reported in the ENSDF [29] with quantum numbers of $J^\pi = 1^-$, whose properties have been determined with different experimental techniques:

- The negative natural parity was determined in an (α, α') experiment by Davis [63].
- Since the energy resolution of the (α, α') experiment was poor compared to gamma-ray spectroscopy, the excitation energy was not measured, but taken from two previous β^--decay studies of ^{40}Cl [64, 65], compiled in Ref. [66].
- Moreh *et al.* [38] reported a dipole-excited state at 5393(3) keV from their NRF experiment and determined an elastic cross section.

Although the energy from the NRF measurement is in disagreement with the β-decay studies, the evaluator of Ref. [29] merged the properties from the aforementioned three different experiments into a single state at 5400.5(8) keV with the quantum numbers $J^\pi = 1^-$ and the level width from Ref. [38]. In the present experiment, the excitation energy of the state of interest was determined to 5391.9(7) keV by an energy calibration relative to two well-known excited states of ^{27}Al and ^{208}Pb (see TABLE II). No signal from an excited state at about 5400 keV was observed. If it were a dipole-excited state, it can be estimated from the background in the spectra of the present experiment (using Eq. (16) and (17) with the reference state at 5392 keV, see also subsection III B 1) that its elastic cross section is at least a factor of 4 lower than the one for the state at 5392 keV. It is probable that the (α, α') experiment has observed the state at about 5392 keV, whose excitation energy has been determined independently by Moreh et al. [38] and the present experiment. Furthermore, the asymmetry is

slightly more in favor of a $J^\pi = 1^-$ assignment and, as discussed later, electric dipole strength is dominant over almost the entire energy range of the present experiment. Due to these arguments, the state at 5392 keV will be treated as an E1 excitation in the following, though we emphasize again the puzzling discrepancy with the energy assignment from the β-decay data.

D. Summary

The results of the analysis are summarized in TABLE II. In total, 20 excited states of ^{40}Ar have been observed. The majority of those, 15, are electric dipole-excited states, which make up more than 85 % of the elastic cross section of resolved transitions. Two states have been identified unambiguously as magnetic dipole-excited states, while three more states are also most favorably populated by this electromagnetic character. For one state at 5392 keV, previously assigned $J^\pi = 1^-$ [29], the parity quantum number could not be unambiguously confirmed by this experiment due to low statistics (see the discussion in subsection III C 1).

IV. DISCUSSION

After the presentation of the experimentally accessible quantities in the previous section, this section discusses the impact of the experimental sensitity limit and attempts to establish a lower and upper limit for the observed magnetic dipole strength. First, the directly observed strength is compared to the shell model calculation of Ref. [35] in subsection IV A. The comparison will pose the question whether there is additional magnetic dipole strength which could not have been observed with the given sensitivity limit. Estimates for the amount of unobserved branching transitions and ground-state transitions will be given in subsections IV B and IV C, respectively.

A. Comparison to Shell Model

In Ref. [35], Li *et al.* noted the agreement of their single observed $M1$ excitation with a shell model calculation in the *sd-fp* model space [36]. It was used to interpret the state at 9757 MeV as a fragment of the proton $d_{5/2} \rightarrow d_{3/2}$ spin-flip. Concerning the motivation of this work, this would confirm that a separation of the orbital and the spin-part of the isovector $M1$ operator in Eq. (6) by nuclear theory is possible.

Since the shell model calculation predicts a larger part of the magnetic dipole strength at lower energies, the results of this experiment can be used to improve the experimental constraints. For the comparison of the combined $M1$ strength distribution measured in both experiments to the same calculation, which is shown in FIG. 3, the measured elastic integrated cross sections for single states were converted to the quantity

$$\mathfrak{B}(\lambda L; 0_1^+ \rightarrow 1_i^+) \equiv \frac{\Gamma_{i\rightarrow 0}}{\Gamma_i} \mathrm{B}(\lambda L; 0_1^+ \rightarrow 1_i^+) \propto I_{0\rightarrow i\rightarrow 0} \tag{21}$$

using Eqs. (8)-(14). The ground-state branching ratio $\Gamma_{i\rightarrow 0}/\Gamma_i$ in Eq. (21) takes into account the impact of unobserved decay transitions. The quantity $\mathfrak{B}(\lambda L)\uparrow$ provides a lower limit for the excitation strength $\mathrm{B}(\lambda L)\uparrow$ by definition and equals this excitation strength if the ground-state decay is predominant. Considering the individual states, the onset of the observed strength and the location of the strongest fragments is described well. Indeed, the 1^+ state with the largest observed $M1$ excitation strength resides near 4.5 MeV excitation energy as predicted by theory [35]. The total $M1$ strength predicted by the shell model $B(M1; 0_1^+ \rightarrow 1^+)_{\mathrm{sm}}$ and the total observed strength $\mathfrak{B}(M1; 0_1^+ \rightarrow 1^+)_{\mathrm{exp}}$ are obtained by summing up the transition strengths of individual states i up to 11 MeV, corresponding to the experimental energy range. It was found that $B(M1; 0_1^+ \rightarrow 1^+)_{\mathrm{sm}} = 0.835\,\mu_{\mathrm{N}}^2$ [3], indicated by the running sum in the figure, is about a factor of 1.5 larger than the directly observed $\mathfrak{B}(M1; 0_1^+ \rightarrow 1^+)_{\mathrm{exp}} = 0.50(7)\,\mu_{\mathrm{N}}^2$. Furthermore, the predicted excitation strength of the first excited 1^+ level at about 4.5 MeV, which is both the strongest excited state in this experiment and in the shell model, is overestimated by more than a factor of two. Considering that the cross section for low-energy neutrino scattering [28] is an inversely energy-weighted sum of $B(GT)$ strength (lower-lying states have a higher weight), the overestimation of the excitation strength of this state is particulary unsatisfactory. The observed discrepancies may be caused both by the experimental method and deficiencies of the model.

Since this is an experimental publication, the following sections will be dedicated to the estimation of an upper limit for the experimentally observed strength. The two contributions to systematic uncertainties in NRF experiments are unobserved branching transitions as shown in Eqs. (8) and (21), and ground-state transitions below the sensitivity limit which will be labeled 'sl' in the following. Especially in recent discussions about low-lying electric dipole strength [46], it was shown that these two factors need to be under control in order to compare NRF state-to-state analyses to measurements or predictions of the total photoabsorption cross section [68, 69]. Both can be introduced as corrections to $\mathfrak{B}(M1; 0_1^+ \rightarrow 1^+)_{\mathrm{exp}}$ to obtain the total strength:

$$\mathrm{B}(M1; 0_1^+ \rightarrow 1^+) = \sum_i \frac{\Gamma_i}{\Gamma_{0\rightarrow i}} \mathfrak{B}(M1; 0_1^+ \rightarrow 1_i^+)_{\mathrm{exp}} + \sum_j \mathrm{B}(M1; 0_1^+ \rightarrow 1_j^+)_{\mathrm{sl}}. \tag{22}$$

[3] It should be noted that the shell model already utilized a typical quenching factor of 0.7 for the spin g-factors in Eq. (6).

TABLE II. Properties of dipole- and quadrupole-excited states of ^{40}Ar between 4.2 and 7.7 MeV observed in this experiment. Newly observed states are marked by an asterisk in the first column. Elastic cross sections and level energies were taken from the publication by Moreh *et al.* [38] if not indicated otherwise. This reference actually gives values of $g\Gamma_0^2/\Gamma$, which were converted to an elastic scattering cross section using Eq. (8). For the conversion of elastic cross sections to transition strengths, $\Gamma_0/\Gamma = 1$ was assumed in all cases where no branching transition was known in the literature [29]. In the case of the transition at 6100 keV, the present result for the branching ratio agreed so well with the one quoted by Moreh et al. [38], that $\mathfrak{B}(E1)\uparrow$ was calculated using their branching ratio. Excitation energies of newly observed states were inferred from known energies [29] of other transitions in the same beam spectrum. Their uncertainty is a combination of the uncertainty of the excitation energies of the reference states and the internal energy resolution of the HPGe detectors. The latter limits the precision of the determined peak position of the approximately Gaussian lineshape. The gamma-ray energies which correspond to unobserved transitions were calculated from the excited-state energies in the first column and from the literature value of the energy of the first excited 2^+ state [29]. All reported branching transitions and upper limits have been determined in this work. Upper limits for unobserved branching transitions and multipole orders higher than the lowest allowed one have been neglected to obtain $\mathfrak{B}(E1)\uparrow$ and $\mathfrak{B}(M1)\uparrow$ from the given elastic cross section. Their relation to the actual reduced transition strength $B(\lambda L)$ is described in the context of Eq. (21).

E_i keV	E_γ keV	Asymmetry	$J_i^{\pi i}$	$J_f^{\pi f}$	$\Gamma_{i\to f}/\Gamma$	$I_{0\to i\to 0}$ eVb	$\mathfrak{B}(E1)\uparrow$ $10^{-3}e^2\mathrm{fm}^2$	$\mathfrak{B}(M1)\uparrow$ μ_N^2
4473(1) [a]	4473(1)	$0.77^{+0.12}_{-0.12}$	1^+	0_1^+	1	40(8)		$0.21^{+0.04}_{-0.04}$
	3012(1)			2_1^+	< 0.08			< 0.0137
5391.9(7) [b]	5393(3)	$-0.2^{+0.4}_{-0.4}$	1^- [c]	0_1^+	1	11.9(26)	$0.5^{+0.099}_{-0.14}$	$0.046^{+0.009}_{-0.012}$ [c]
	3932(3)			2_1^+	< 0.9		< 12.0	< 1.1 [c]
5656(3)*	5656(3)	$-0.62^{+0.16}_{-0.13}$	1^-	0_1^+	1	15.1(34)	$0.6^{+0.15}_{-0.16}$	
	4195(3)			2_1^+	< 0.5		< 0.5	
5850(3)*	5850(3)	$0.29^{+0.5}_{-0.46}$	$1^+, (2^+)$	0_1^+	1	2.8(7)		$0.0101^{+0.0025}_{-0.0036}$
	4389(3)			2_1^+	< 0.7			< 0.037
5880.3(4) [a]	5880.3(4)	$-0.85^{+0.05}_{-0.05}$	1^-	0_1^+	$0.74^{+0.06}_{-0.04}$ [d]	39(4)	$1.95^{+0.46}_{-0.32}$	
	4419.5(4)			2_1^+	< 0.12		< 0.12	
6053.6(8) [a]	6053.6(8)	$-0.843^{+0.032}_{-0.04}$	1^-	0_1^+	1	130(20)	$5.0^{+0.8}_{-0.9}$	
	4592.8(8)			2_1^+	< 0.07		< 0.22	
6083.5(9)	6083.5(9)	$0.51^{+0.09}_{-0.12}$	$1^+, (2^+)$	0_1^+	1	10.1(23)		$0.039^{+0.008}_{-0.007}$
	4622.7(9)			2_1^+	< 0.5			< 0.026
6100(2) [a]	6100(2)	$-0.72^{+0.09}_{-0.07}$	1^-	0_1^+	$0.29^{+0.022}_{-0.029}$	18(5)	$2.8^{+0.8}_{-0.7}$	
	4639(2)			2_1^+	$0.71^{+0.022}_{-0.029}$		$2.6^{+0.6}_{-1.1}$	
6283.8(16)*	6283.8(16)	$-0.61^{+0.29}_{-0.3}$	1^-	0_1^+	1	8.9(29)	$0.34^{+0.15}_{-0.15}$	
	4823.0(16)			2_1^+	< 0.8		< 3.2	
6338.7(11) [a]	6338.7(11)	$-0.85^{+0.06}_{-0.05}$	1^-	0_1^+	1	83(10)	$3.2^{+0.33}_{-0.4}$	
	4877.9(11)			2_1^+	< 0.12		< 0.21	
6476.0(8) [a]	6476.0(8)	$-0.767^{+0.038}_{-0.033}$	1^-	0_1^+	1	118(15)	$5.0^{+0.6}_{-0.5}$	
	5015.2(8)			2_1^+	< 0.07		< 0.16	

[a] Uncertainty from most recent ENSDF evaluation [29].
[b] Uncertainty from energy calibration which used the state of ^{27}Al at 5432.8(10) keV [60] and the 1^- state of ^{208}Pb at 5291.90(12) keV [67].
[c] Parity from most recent ENSDF evaluation [29]. It is not completely sure whether the reported parity actually belongs to this state (see the discussion in the text), therefore the alternative magnetic dipole strength is also given in the ninth column.
[d] Four transitions to excited states which are higher in energy than the 2_1^+ are reported in the most recent ENSDF evaluation [29]. They have been used in the calculation of branching ratios, cross sections, and transitions strengths.

Since only ground-state transitions of 1^+ states have been observed in the present experiment, the correction factor for the branching ratio in Eq. (22) has been simplified to the ratio of the total level width and the partial transition width to the ground state.

The following subsections IV B and IV C discuss the two sums in Eq. (22) separately, starting with the unobserved branchings.

B. Unobserved Branching Transitions

Three different approaches were used in this work to estimate the influence of unobserved branchings:

- An upper limit for direct decays to the 2_1^+ state at 1461 keV [29] was determined which constrains at least one decay branching.

TABLE II. (*continued*)

E_i keV	E_γ keV	Asymmetry	$J_i^{\pi_i}$	$J_f^{\pi_f}$	$\Gamma_{i\to f}/\Gamma$	$I_{0\to i\to 0}$ eVb	$\mathfrak{B}(E1)\uparrow$ $10^{-3}e^2\mathrm{fm}^2$	$\mathfrak{B}(M1)\uparrow$ μ_N^2
6566.2(9)*	6566.2(9)	$-0.74^{+0.09}_{-0.08}$	1^-	0_1^+	1	26(5)	$0.96^{+0.19}_{-0.22}$	
	5105.4(9)			2_1^+	< 0.34		< 0.31	
6921.6(14)* [a]	6921.6(14)	$-0.33^{+0.23}_{-0.21}$	1^-	0_1^+	1	8(5)	$0.27^{+0.19}_{-0.2}$	
	5460.8(14)			2_1^+	< 0.6		< 0.5	
7190(3)*	7190(3)	$-0.74^{+0.16}_{-0.16}$	1^-	0_1^+	1	11.2(28)	$0.4^{+0.09}_{-0.11}$	
	5729(3)			2_1^+	< 0.6		< 0.5	
7246(3) [a]	7246(3)	$0.79^{+0.12}_{-0.13}$	1^+	0_1^+	1	27(5)		$0.087^{+0.019}_{-0.013}$
	5785(3)			2_1^+	< 0.28			< 0.0168
7271(3)*	7271(3)	$0.31^{+0.36}_{-0.28}$	$1^+, (2^+)$	0_1^+	1	4.0(18)		$0.011^{+0.005}_{-0.006}$
	5810(3)			2_1^+	< 0.8			< 0.12
7281(3)	7281(3)	$-0.78^{+0.07}_{-0.06}$	1^-	0_1^+	1	35(7)	$1.1^{+0.22}_{-0.27}$	
	5820(3)			2_1^+	< 0.19		< 0.13	
7519(3) [a]	7519(3)	$-0.76^{+0.09}_{-0.08}$	1^-	0_1^+	1	31(7)	$1.1^{+0.24}_{-0.2}$	
	6058(3)			2_1^+	< 0.29		< 0.23	
7626(3) [a]	7626(3)	$-0.89^{+0.09}_{-0.09}$	1^-	0_1^+	1	22(5)	$0.7^{+0.19}_{-0.15}$	
	6165(3)			2_1^+	< 0.35		< 0.23	
7708(3) [a]	7708(3)	$-0.81^{+0.05}_{-0.05}$	1^-	0_1^+	1	141(21)	$4.0^{+0.6}_{-0.8}$	
	6247(3)			2_1^+	< 0.12		< 0.25	

[a] Uncertainty from energy calibration which used the state of ^{27}Al at 6820.7(13) keV [60].

- The observed depopulation of the 2_1^+ state was used to obtain an average branching ratio of all excited states in an excitation energy window defined by the beam width. This quantity is frequently used to correct photoabsorption cross sections [42, 44–46, 48] from NRF measurements for unobserved branching transitions.

- General properties of the photon strength function (PSF) [70] were employed to establish a phenomenological upper limit.

They will be discussed in the following three subsections IV B 1, IV B 2, and IV B 3 in the given order. Since the first two estimates are both based on the experimental data of this publication, a comparison will be made in the last paragraph of subsection IV B 2 (IV B 2 f).

1. *Direct Decays to the 2_1^+ State*

The upper limits for direct decays to the 2_1^+ were determined according to Eq. (16). For the state observed by Li *et al.* [35], an upper limit for the branching ratio of 10 % was estimated by comparison to the upper limit for the strongly excited 1^+ state at 4473 keV (see TABLE II). Then, it was assumed that the unobserved branchings to the 2_1^+ state are exactly equal to their upper limit for each state to get a first estimate:

$$\frac{\Gamma_i}{\Gamma_{i\to 0}} \approx 1 + \frac{\Gamma_{i\to 2_1^+}}{\Gamma_{i\to 0}} < 1 + \frac{2.3\sqrt{A^{\mathrm{bg}}_{i\to 2_1^+}}}{C_{0\to i\to 2_1^+}(E_i, 1461\,\mathrm{keV})\, I_{0\to i\to 0}}. \tag{23}$$

Eq. (23) was obtained by combining Eqs. (7), (8), and (16), with the abbreviation introduced in Eq. (17). Using the approximation of Eq. (23) in Eq. (22), while neglecting the states below the sensitivity limit, the total experimental $M1$ strength is enhanced by a factor of 1.3 . In principle, it is possible to avoid the initial approximation in Eq. (23) and determine a similar upper limit for every possible decay to a lower-lying excited state. However, the constraints by the sensitivity limit would become increasingly meaningless, because it can be anticipated from the experimental spectra and the measured detection efficiencies that the factor

$$\frac{A^{\mathrm{bg}}_{i\to f}}{C_{0\to i\to f}(E_i, E_f)}, \tag{24}$$

which would appear in analogy to Eq. (23), increases monotonously with increasing E_f.

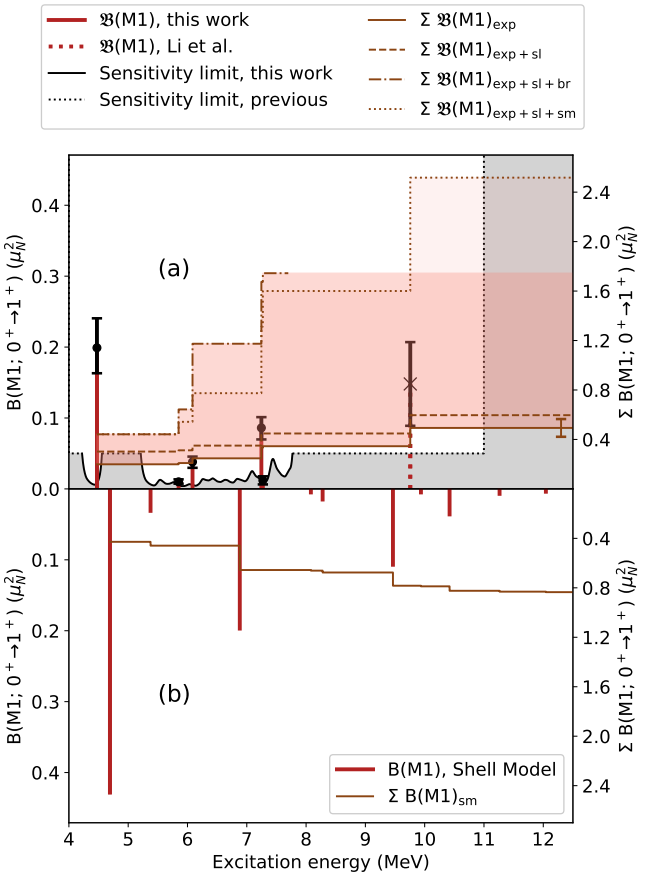

FIG. 3. Comparison of the observed $M1$ strength to a shell model calculation from Ref. [35]. The observed (a) and calculated (b) reduced excitation strengths of single states are shown as red bars, with an error bar on top for the experimental values. A combined sensitivity limit of this work, Li *et al.* [35], and Moreh et al. [38] is shown as a grey-shaded area. The running sum over the depicted magnetic dipole strength is shown as a brown line, including an error bar for the experiment. Unobserved $M1$ strength has been estimated by taking into account the sensitivity limits (*sl*), and unobserved branchings, either by experimental average branching ratios (*br*) or by a statistical model calculation (*sm*). Since no average branching ratios were determined by Li *et al.* [35], the corresponding line ends at the energy range of the present experiment. The effects of all estimates on the running sum are shown as dotted, dashed, and dash-dotted brown lines, respectively, and by the red-shaded transparent areas. Note the different scale of the y-axis for individual and accumulated $M1$ strength.

2. *Observed Population of the* 2_1^+ *State*

The second method to estimate the amount of unobserved branchings uses the observed number of decays of the 2_1^+ state of ^{40}Ar. It was discussed in section III A that this is often assumed to be a good approximation for the total number of decays to lower-lying excited states. Some additional definitions for the correction of the observed strength by the observed average branching are introduced in paragraph IV B 2 a. After that, the subtraction of the background contamination of the $2_1^+ \to 0_1^+$ transition is described (paragraph IV B 2 b). Using the number of events in the $2_1^+ \to 0_1^+$ transition, which is very probably fed by cascades from 1^+ and 1^-, a conservative but model-independent upper-limit estimate is obtained in paragraph IV B 2 d by attributing all of them to 1^+ states. In addition, the experimental asymmetry of this transition is taken into account in a model-dependent way in section IV B 2 e to refine this limit [43]. The two different possibilities are compared in paragraph IV B 2 f.

a. Definitions Since the quantity $\sum_i I_{i\Rightarrow 2_1^+}$ from Eq. (12) can be used to approximate the average ground-state branching $\langle b_0 \rangle$ (Eq. (12)), the aim is to give a relation between the total strengths $B(M1; 0_1^+ \to 1^+)$ and $\mathfrak{B}(M1; 0_1^+ \to 1^+)$. The derivation starts by inserting the definition of $I_{0\to i\to 0}$ (Eq. (8)) and Γ_0 into the definition of $\langle b_0 \rangle$ (Eq. (11) and (13)):

$$\langle b_0(J^\pi) \rangle = \frac{\sum_i \frac{(2J_i+1)(L+1)}{L[(2L+1)!!]^2} \left(\frac{E_i}{\hbar c}\right)^{2L+1} B(\lambda L; 0 \to J_i^\pi) \frac{\Gamma_{0\to i}}{\Gamma_i}}{\sum_i \frac{(2J_i+1)(L+1)}{L[(2L+1)!!]^2} \left(\frac{E_i}{\hbar c}\right)^{2L+1} B(\lambda L; 0 \to J_i^\pi)}. \quad (25)$$

In Eq. (25), the angular momentum of the ground state has already been inserted. This restricts the sum over possible multipolarities to a single value. The dominance of dipole excitations ($J_i = L = 1$, or $\langle b_0 \rangle \gtrapprox \langle b_0(1^+) \rangle + \langle b_0(1^-) \rangle$) and $E_i \approx E_{\text{beam}}$ can be assumed to simplify the equation, since only dipole-excited states were observed and the width of the beam profile was small compared to the excitation energy. In this case, most of the constant factors cancel out:

$$\langle b_0(1^\pi) \rangle \approx \frac{\sum_i B(\lambda 1; 0 \to 1_i^\pi) \frac{\Gamma_{0\to i}}{\Gamma_i}}{\sum_i B(\lambda 1; 0 \to 1_i^\pi)}. \quad (26)$$

Eq. (26) can be solved for the denominator, which is the total excitation strength with electromagnetic character λ:

$$\begin{aligned} B(\lambda 1; 0 \to 1^\pi) &\equiv \sum_i B(\lambda 1; 0 \to 1_i^\pi) \\ &= \frac{1}{\langle b_0(1^\pi) \rangle} \sum_i B(\lambda 1; 0 \to 1_i^\pi) \frac{\Gamma_{0\to i}}{\Gamma_i} \\ &\overset{\text{Eq. (21)}}{=} \frac{1}{\langle b_0(1^\pi) \rangle} \mathfrak{B}(\lambda 1; 0 \to 1^\pi) \\ &\geq \frac{\sum_i I_{0\to i\to 0} + \sum_i I_{i\Rightarrow 2_1^+}}{\sum_i I_{0\to i\to 0}} \mathfrak{B}(\lambda 1; 0 \to 1^\pi). \end{aligned} \quad (27)$$

Note that the last term in Eq. (27), which was obtained by inserting inequality (13), contains only experimental observables. In the derivation, unobserved ground-state transitions have been neglected in accordance with the discussion in section III A. Since the separation of

$\langle b_0(1^+)\rangle$ and $\langle b_0(1^-)\rangle$ depends on the assumption of a dominant direct branching to the 2_1^+ state, and the experiment is not very sensitive to the two contributions, we will later resort to the model-independent upper limit which uses $\langle b_0\rangle > \langle b_0(1^\pi)\rangle$.

No other decays of lower-lying excited states were observed in the spectra according to the sensitivity limit of Eq. (16). However, the known branching ratios [29] suggest that even most cascades starting from low-lying states will end up populating the 2_1^+ state, which confirms the assumed 'funnel-effect' of the 2_1^+ state.

b. Background subtraction For the particular case of ^{40}Ar, events in the spectra at the energy of the $2_1^+ \to 0_1^+$ transition at 1461 keV are not caused by gamma rays following excitation via NRF only, but also by decay of naturally occurring ^{40}K to ^{40}Ar [29]. Large abundances of potassium are contained in the walls and floor of the Upstream Target Room (UTR) at HIγS, so that this background amounted to more than 50 % of the counted events with an energy of 1461 keV. It was possible to extract the NRF events by subtracting the spectra of the empty bottle or the ^{56}Co source which were normalized using two background lines at 1765 keV from ^{214}Po [71] and 2615 keV from ^{208}Pb [67]. In the case that both empty-bottle and source spectra were available, the former were preferred, because the geometry was exactly equal to the ^{40}Ar measurements, while for the source measurements, the gas bottle was removed.

c. Asymmetry of the $2_1^+ \to 0^+$ transition Depending on the cascade that populated the 2_1^+ state, the decay to the ground state can be expected to exhibit an asymmetry $\epsilon_{2_1^+}$, which is less pronounced than for $0^+ \to 1^\pm \to 0^+$ cascades. For a direct population of the 2_1^+ state from 1^+ (1^-) states, the asymmetry of the $2^+ \to 0^+$ transition is $\epsilon_{1^+\to 2_1^+} = -0.33$ ($\epsilon_{1^-\to 2_1^+} = 0.33$) if the dimensions of the target and the detectors are negligible. For the geometry of the present experiment, $\epsilon^{\text{sim}}_{1^+\to 2_1^+} = -0.30$ ($\epsilon^{\text{sim}}_{1^-\to 2_1^+} = 0.25$) is expected from GEANT4 simulations [9–11]. The absolute value of $\epsilon_{2_1^+}$ decreases rapidly with an increasing number of intermediate steps of the cascade [40]. The observed asymmetries of the $2_1^+ \to 0^+$ transition for all beam energies are shown in part (b) of FIG. 4. Within a 2σ interval, none of them is significantly different from an isotropic decay, indicating that indirect gamma-decay channels are in competition with the direct population of the 2_1^+. This is especially obvious for the beam energy of 4.44(FWHM: 0.19) MeV, where the asymmetry is most probably positive, although only a single 1^+ state was observed. Possible indirect decays via an intermediate state with $J = 0, 1$ or 2, with ideal asymmetries of $\epsilon_{2_1^+} = 0, 0.2$ and -0.18, respectively, or a multipole mixing ratio with $|\delta| > 0.4$ for the $1^+ \to 2_1^+$ decay, would be the most obvious deviations from the assumed direct decay which are in agreement with the experimental asymmetry within a 90 % confidence interval.

d. Average branching of dipole-excited states From the observed counts of NRF events of the $2_1^+ \to 0_1^+$ transition, an estimate for the average branching to lower-lying excited states ($1 - \langle b_0\rangle$) was determined using Eq. (11) and (12) as described above. To obtain $I_{i\Rightarrow 2_1^+}$ in Eq. (12), the angular distribution of the decay of the 2_1^+ state was assumed to be isotropic, which is in accordance with almost all observed asymmetries. Since the observed NRF events are the sum of $I_{1^+\Rightarrow 2_1^+}$ and $I_{1^-\Rightarrow 2_1^+}$[4], and a separation is not possible without further assumptions, $\langle b_0\rangle$ instead of a specific $\langle b_0(1^\pi)\rangle$ was used in Eq. (27) to obtain an upper limit of the total resolved $M1$ strength. The values of $1 - \langle b_0\rangle$ are shown as error bars in part (a) of FIG. 4. For each beam energy, two data points are shown. They represent the upper limit where the complete population of the 2_1^+ state is attributed to 1^+ or 1^- states, respectively. For the observed 1^+ states, the estimates indicate that the total level width Γ_i in Eq. (21) may be larger than $\Gamma_{0\to i}$ by more than a factor of 3. The quantity $^1/_{\langle b_0\rangle}\mathfrak{B}(M1, 0 \to 1^+)$ is shown in FIG. 3 as a dash-dotted line which ends at the energy range of this experiment (7.7 MeV).

e. Average branching of 1^+ and 1^- states Although it is probable from the observed asymmetries that the 2_1^+ state is populated by multi-step cascades as well, an attempt was made to separate the NRF events N of the $2_1^+ \to 0_1^+$ transition into contributions from $1^+ \to 2^+$ ($N_{1^+\to 2^+}$) and $1^- \to 2^+$ ($N_{1^-\to 2^+}$) cascades using the simulated asymmetries $\epsilon^{\text{sim}}_{1^+\to 2_1^+}$ and $\epsilon^{\text{sim}}_{1^-\to 2_1^+}$ for pure multipole character ($\delta = 0$). For this, the following relation was used, which follows from Eq. (19):

$$\frac{N_{1^-\to 2_1^+}}{N_{1^+\to 2_1^+}} = \frac{\epsilon^{\text{sim}}_{1^+\to 2_1^+} - \epsilon_{2_1^+}}{\epsilon_{2_1^+} - \epsilon^{\text{sim}}_{1^-\to 2_1^+}}. \tag{28}$$

In Eq. (28), it was assumed that the lowest multipole order dominates, i.e. $\delta = 0$ for the $1^\pm \to 2_1^+$ transition. The separation reduces the estimated number of decays via intermediate states, therefore $1 - \langle b_0(1^\pi)\rangle < 1 - \langle b_0\rangle$. The values of $1 - \langle b_0(1^\pm)\rangle$ are shown in part (c) of Fig. 4.

For the beam energy of 4.44(FWHM: 0.19) keV, the result is most easily understood: The decay of the 2_1^+ state of ^{40}Ar was observed, that means it must have been populated from some higher-lying excited state that was initially populated by the beam. Only a single 1^+ state has been observed in this energy region in the present experiment, therefore $1 - \langle b_0\rangle = 0.41^{+0.07}_{-0.18}$ was obtained for 1^+ states in paragraph IV B 2 d. However, the asymmetry of the $2_1^+ \to 0_1^+$ transition is in perfect agreement with a direct population by initially excited 1^- states. Therefore, the additional assumption of this paragraph attributes all

[4] In accordance with the discussion in Section III C, the impact of electric quadrupole strength will be neglected in this one and the following paragraph.

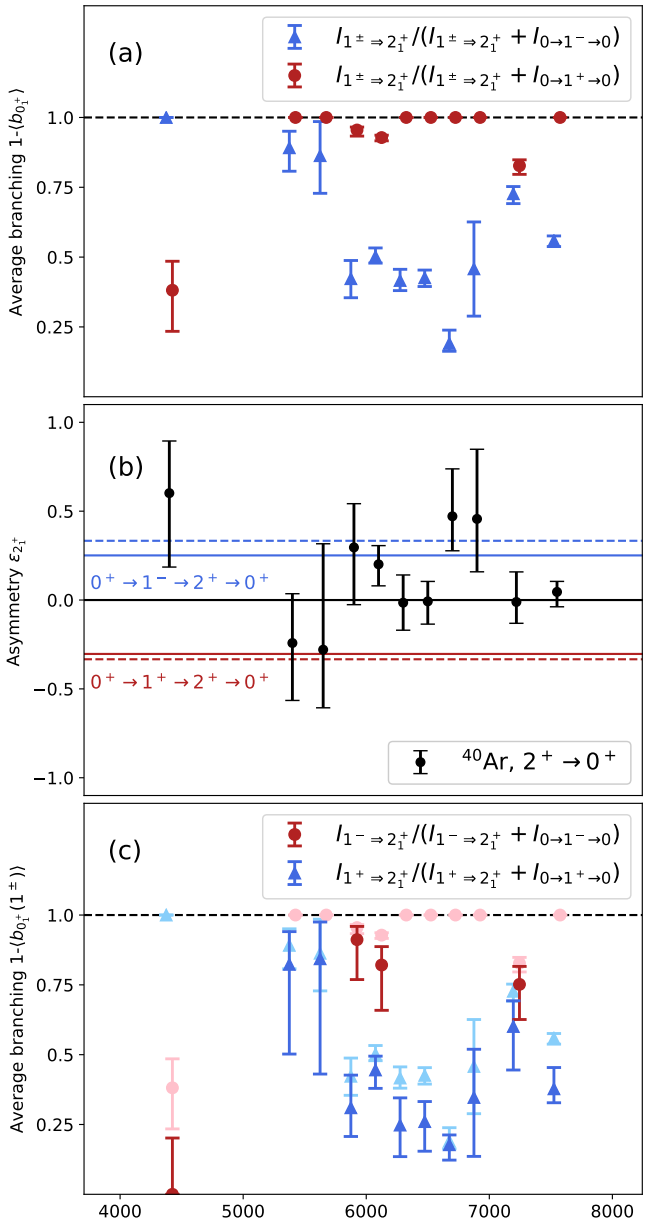

FIG. 4. (a) Average branching of dipole-excited states to lower-lying excited states, estimated using the counts of the $2_1^+ \to 0_1^+$ transition (Eq. (12) in (11)). A value of $1 - \langle b_{0_1^+} \rangle = 1$ means that no discrete dipole-excitated states with this electromagnetic character were observed at the given energy. (b) Count-rate asymmetry $\epsilon_{2_1^+}$ of the $2_1^+ \to 0_1^+$ transition of ^{40}Ar for each beam energy setting. The expected asymmetries for a direct population of the 2_1^+ state by M1 (E1) transitions from 1^+ (1^-) states are shown as red (blue) lines. The dashed lines indicate the ideal asymmetry, while the solid lines take into account the geometry of the target and the detectors. (c) Average branching $\langle b_{0_1^+}(1^\pm) \rangle$ of 1^+ and 1^- states, obtained from (a) and (b) using the assumption that direct decays ($1^\pm \to 2_1^+$) dominate (Eq. (28)). The values of $\langle b_{0_1^+} \rangle$ from (a) are shown in lighter colors for comparison.

the inelastic decays to 1^- states and $1 - \langle b_0(1^+) \rangle = 0^{+0.20}_{-0}$ is consistent with zero.

Due to the strong assumption of single-step population, the extended error bars are to be seen as an order-of-magnitude estimate only. In all of the following argumentation, 'average branching' will refer to the un-separated value of $1 - \langle b_{0_1^+} \rangle$.

f. Discussion of experimental branching estimates It is now possible to compare the experimental estimates of the unobserved branching ratios from paragraphs IV B 1 and IV B 2 d, which use the quantities $\Gamma_{i \to 2_1^+}/\Gamma_i$ (TABLE II) and $1 - \langle b_0 \rangle$ (FIG. 4), respectively. With few exceptions where strongly excited 1^- states dominate the average branching, $1 - \langle b_0 \rangle > \Gamma_{i \to 2_1^+}/\Gamma_i$. For example, at a beam energy of 4.44(FWHM:0.19) keV, the upper limit for direct decays of the 1^+ state at 4473 keV to the 2_1^+ state is $\Gamma_{i \to 2_1^+}/\Gamma_i < 0.08$, while $1 - \langle b_0 \rangle < 0.48$. That means the upper limit for the average branching ratio allows for a much higher amount of inelastic decays as would be expected from the upper limits of the decays to the 2_1^+ state, indicating that there could be significant unobserved branching to higher-lying excited states.

As noted before, a correction to $\mathfrak{B}(M1; 0_1^+ \to 1^+)$ by the average branching ratio is shown in FIG. 3 as a dash-dotted line. Note that this correction could still change in both directions: If the major part of the population of the 2_1^+ state was from 1^- states, the correction would decrease. On the other hand, if the assumed 'funnel-effect' of the 2_1^+ state is incorrect, the correction would increase.

3. *Phenomenological Strength Function*

In a third approach, a constraint will be obtained from a model for the photon strength function (PSF) [70]

$$\overleftarrow{f}_{\lambda \mathrm{L}}(E_i - E_f) = \frac{\langle \Gamma_{i \to f} \rangle \rho(E_i, J_i, \pi_i)}{(E_i - E_f)^{2L+1}}, \qquad (29)$$

which describes the average photoemission properties of a nucleus. It depends on the average partial widths $\langle \Gamma_{i \to f} \rangle$ of transitions from states at energies E_i to $E_f < E_i$ and the nuclear level density $\rho(E_i, J_i, \pi_i)$ at the energy of the decaying states. The latter has already been restricted to states with a certain set of quantum numbers $J_i^{\pi_i}$. Eq. (29) shows the so-called 'downward' PSF $\overleftarrow{f}_{\lambda \mathrm{L}}$. In general, it does not have to be equal to the 'upward' PSF $\overrightarrow{f}_{\lambda \mathrm{L}}$, which describes the average photoabsorption capability of the nucleus (see, e.g. Ref. [72]). Especially for the $E1$ and $M1$-PSF from the ground state ($E_f = 0$), widely used parameterizations exist [73]. A set of transition widths between states of a nucleus can be interpreted as one possible sample drawn from a distribution whose average value is given by the PSF [70]. Depending on the sample size, it may be subject to strong fluctuations, which are often assumed to follow a chi-squared distribution with one degree of freedom (χ^2_1 or Porter-Thomas)

distribution [74]. Therefore, the statistical model [75] is mostly applied in regions of high level densities. For the nucleus ^{40}Ar, which is close to the doubly magic shell closure at ^{40}Ca, it can be expected that a statistical treatment of decay properties is valid only for higher excitation energies at the upper limit of the present experiment. From the definition in Eq. (29), an expression for the average transition width to excited states can be derived. To obtain the partial transition widths from a 1^+ state to all excited states above the 2_1^+ state, one would have to calculate the sum over all intermediate excited states of ^{40}Ar for all possible multipolarities. Since low multipolarity usually dominates gamma-ray transitions between nuclear states, the sum is restricted to the electric and magnetic dipole strength functions. Furthermore, $\langle\Gamma_{i\to f}\rangle$ is treated as a continuous function of the energy to obtain simple results. This way, unobserved intermediate states can be taken into account by a model of the level density. Anticipating the results given in Eq. (30) and (32), note that the absolute value of the level density will cancel out, and that most phenomenological models for $\rho(E)$ [73] agree on an overall exponential increase with energy. The sum of all transition widths from a state i to all lower-lying states j in the energy range between states f and g with $E_f \geq E_j \geq E_g$ is then given by:

$$\begin{aligned}\sum_{j;E_f\geq E_j\geq E_g}\langle\Gamma_{i\to j}\rangle \approx & \frac{2}{f(1)\rho(E_i)}\left[\sum_{j;E_f\geq E_j\geq E_g}\left\{f_{E1}(E_i-E_j)\left(1-\delta_{\pi_i\pi_j}\right)+f_{M1}(E_i-E_j)\delta_{\pi_i\pi_j}\right\}(E_i-E_k)^3\right] \\ \xrightarrow{\sum_j\gg 1} & \frac{f(0)+f(1)+f(2)}{f(1)\rho(E_i)}\left[\int_{E_i-E_f}^{E_i-E_g}\{f_{E1}(E_\gamma)+f_{M1}(E_\gamma)\}E_\gamma^3\rho(E_i-E_\gamma)\mathrm{d}E_\gamma\right].\end{aligned} \tag{30}$$

In the first step, the definition of the PSF has been inserted for discrete states, and the restriction to dipole transitions has been applied. The two δ-functions which compare the parities of the initial and final states implement the restriction to a single electromagnetic character for a given transition [33]. According to Ref. [76], the angular momentum-, parity-, and energy-dependent part of the level density are separable:

$$\rho(E,J,\pi)=\frac{1}{2}f(J)\rho(E). \tag{31}$$

In Eq. (31), $f(J)$ denotes the distribution of angular momenta, while the distribution of parities is assumed to be equal and creates a factor of one half. Note that due to the approximated energy independence of $f(J)$ and the equal parity distribution, both factors will cancel out in the calculation of branching ratios. In the second step of Eq. (30), the transition to the continuum was executed, which is indicated symbolically as $\sum_j \gg 1$. Note that, compared to the sum over an unknown number of states, the integration includes the density of final states with spin $J=0,1$ and 2, which can be reached by dipole transitions from a dipole-excited state. In the integration, E_γ has been substituted for the energy difference between state i and j, because it can be interpreted as the energy of the emitted γ-ray. For the PSFs in Eq. (30), the forms proposed by Goriely and Plujko [77] were taken, which contain the most prominent features of the dipole response of atomic nuclei. Their parameterizations of $\overleftarrow{f}_{M1}$ also include an upbend at low energies, which was discovered experimentally via the Oslo method [78] and attributed to magnetic dipole transitions by a shell-model analysis [79]. This part of the downward PSF is especially important in the present case, because it would be almost impossible to separate the low-energetic gamma-ray transitions associated with an upbend from nonresonantly scattered photons in an NRF experiment. For the level density, the so-called constant-temperature model [80, 81] with parameters for ^{40}Ar from Ref. [82] was used. Both the model for the PSF and the level density were derived from bulk properties of atomic nuclei. As in the discussion about the interpretation of the PSF in the statistical model, their applicability to the nucleus ^{40}Ar will increase with the excitation energy, since transitions between low-lying levels are strongly influenced by shell structure. Using the models for the PSF and the level density in Eq. (30), the excitation-energy dependent ratio of the transition widths to all excited states below and above 2 MeV was calculated [5]:

$$r(E_i)=\frac{\sum_{j;E_i\geq E_j\geq 2\,\mathrm{MeV}}\langle\Gamma_{i\to j}\rangle}{\sum_{j;2\,\mathrm{MeV}\geq E_j\geq 0}\langle\Gamma_{i\to j}\rangle}. \tag{32}$$

Eq. (32) can be interpreted as the ratio of all transition widths to states above 2 MeV and below 2 MeV (i.e. the 2_1^+ state). It is the factor that has to be applied to the right-hand side of Eq. (23) to restore the equality. The value of the factor r ranges from $r(4\,\mathrm{MeV})=0.3(0.1)$ (meaning that, in this model, states with an excitation energy of 4 MeV have an average branching ratio to the ground state of 77(91) %) to $r(11\,\mathrm{MeV})=8.5(7.5)$, increasing smoothly over the experimental energy range.

[5] Note that the only excited state below 2 MeV in ^{40}Ar is the 2_1^+ state [29]. This is in agreement with the prediction of the level density model.

For the alternative values in parentheses, the upbend of the $M1$-PSF has been neglected. The comparison shows that the effect of the upbend is comparably small at high energies, because low-energetic transitions between close-lying states are suppressed by the gamma energy to the third power. To obtain an upper limit for unobserved branching transitions that also takes into account the transitions to intermediate states besides the 2_1^+ state, the factor $\Gamma_{i\to 2_1^+}$ in Eq. (23) is multiplied by the energy-dependent factor $(1+r)$. This has the potential to enhance the total experimental $M1$ strength by up to a factor of 5. In the energy range of this experiment, the statistical-model estimate of the additional strength agrees with the average-branching estimate within 15 %. In order to determine a limit for the unobserved branchings of the single state observed by Li *et al.*, where no average branching is known, we therefore resort to the statistical model calculation. Since it is the highest-lying 1^+ state in the energy range below the neutron separation threshold, the statistical model should be most likely applicable there.

C. Unobserved Ground-State Transitions

Besides the unobserved branchings, a hypothetical strong fragmentation of the $M1$ strength would add to the continuous background in the range of the beam spectrum, which is otherwise caused by nonresonant elastic scattering of photons off the target and small-angle inelastic scattering along the beamline. A strong fragmentation is indeed anticipated from a shell model study of the argon isotopes ^{36}Ar and ^{38}Ar, which showed that correlations between *sd*- and *pf*-shell configurations are significant despite the semi-magic nature of ^{38}Ar [83]. To estimate the number of weakly excited 1^+ states below the detection limit, we take the shell model calculation from Ref. [35], by the same authors as in Ref. [83], as a reference. Summing the strength of all three predicted states with $B(M1;0\to i)\uparrow_{\mathrm{sm}} < 0.05\,\mu_{\mathrm{N}}^2$, i.e. values below the detection limits of Li *et al.* and Moreh *et al.*, gives a value of $B(M1)\uparrow_{\mathrm{sl}} \approx 0.1\,\mu_{\mathrm{N}}^2$. The detection limit of Moreh *et al.* was set to a value of $0.05\,\mu_{\mathrm{N}}^2$, corresponding to the lowest excitation cross sections that they observed in their experiment. In the small energy range of about 4 MeV to 5 MeV where this estimate was needed, a constant detection limit should not be too far from reality. Note, however, that the detection limits in a bremsstrahlung experiment are actually strongly energy dependent.

The corrections for the unobserved branchings (from the experimental average branching ratios and, if unknown, the statistical model) and ground-state transitions have been added successively to the running sum in FIG. 3, yielding an aggregate upper limit of $\mathrm{B}(M1;0_1^+\to 1^+) \le 2.4\,\mu_{\mathrm{N}}^2$ for the $M1$ excitation strength below 11 MeV excitation energy. Note that this represents a conservative upper limit estimate, especially where the branchings are concerned. Since no transitions of 1^+ states to lower-lying excited states were observed at all, the branching ratios could still be arbitrarily small. Within the large range given by the estimate, the experimental data are in agreement with the shell model calculation that may be considered for separating the orbital and spin part of the magnetic dipole strength (see Eq. (6)) and modeling NC reactions on ^{40}Ar in the energy range studied here. In particular, the predicted $M1$ excitation strength of the lowest-lying excited state is now in agreement with the estimated strength, considering the conservative upper limit.

V. SUMMARY

We have investigated dipole-excitated states of ^{40}Ar below 7.7 MeV with the NRF technique using a quasi-monoenergetic polarized photon beam, completing a previous experimental study which scanned the energy range from 7.7 MeV up to the neutron separation threshold. In total, 20 excited states of this isotope were observed. For most of them, electric or magnetic dipole character was assigned unambiguously with the help of a previous bremsstrahlung experiment. The five magnetic dipole excitations in this energy range were compared to a shell model calculation, which reproduces the energies of the states well. However, the total directly observed strength of $\mathfrak{B}\,(M1)\uparrow = 0.36^{+0.04}_{-0.05}\,\mu_{\mathrm{N}}^2$ in the experiment is lower than predicted. With the knowledge that the observed strength constitutes a lower limit, the sensitivity of the data, the given systematic uncertainties, and well-established PSF models were exploited in a detailed analysis to obtain an upper limit as well. The lower and upper limit restrict the magnetic dipole strength of ^{40}Ar below the neutron separation threshold to $0.5\,\mu_{\mathrm{N}}^2 < B(M1)\uparrow < 2.4\,\mu_{\mathrm{N}}^2$. In their publication from 2007, Lisetskiy *et al.* [83] were not able to perform calculations in the full *sdpf* space due to technical restrictions. It might be instructive to revisit this problem in a less-truncated model space to examine whether the expected increased fragmentation improves the agreement with the experiment. Via the direct proportionality of the strength of spin-flip $M1$ transitions to the NC neutrino interaction cross section, the present work combined with the earlier work of Ref. [35] provides constraints on calculated cross section of solar and supernova neutrinos with ^{40}Ar.

ACKNOWLEDGMENTS

We would like to thank the HIγS accelerator staff for providing excellent experimental conditions. We thank V. Derya, M. Gooden, B. Löher and C. Romig for their contributions to the experiment. We thank A.C. Hayes for fruitful discussions about the implications for NC neutrino scattering. This work was supported by

the Deutsche Forschungsgemeinschaft under Grants No. SFB 634 and SFB 1245 and by the U.S. Department of Energy, Office of Nuclear Physics, under Grant No. DE-FG02-97ER41033. MS, PCR, TB and UG acknowledge support by the Helmholtz Graduate School for Hadron and Ion Research of the Helmholtz Association.

[1] C. Rubbia, The liquid argon time projection chamber: A new concept for neutrino detectors, CERN EP Internal Report **77**, 1 (1977).

[2] C. Rubbia, M. Antonello, P. Aprili, B. Baibussinov, M. B. Ceolin, L. Barzè, P. Benetti, E. Calligarich, N. Canci, F. Carbonara, *et al.*, Underground operation of the ICARUS T600 LAr-TPC: first results, J. Instrum. **6** (7), P07011.

[3] C. Anderson, M. Antonello, B. Baller, T. Bolton, C. Bromberg, F. Cavanna, E. Church, D. Edmunds, A. Ereditato, S. Farooq, *et al.*, The ArgoNeuT detector in the NuMI low-energy beam line at Fermilab, Journal of Instrumentation **7** (10), P10019.

[4] The MicroBooNE Collaboration, Design and construction of the microboone detector, Journal of Instrumentation **12** (02), P02017.

[5] B. Abi, R. Acciarri, M. A. Acero, M. Adamowski, C. Adams, D. L. Adams, P. Adamson, M. Adinolfi, Z. Ahmad, C. H. Albright, *et al.*, The Single-Phase ProtoDUNE Technical Design Report (2017), arXiv:1706.07081.

[6] R. Acciarri, M. A. Acero, M. Adamowski, C. Adams, P. Adamson, S. Adhikari, Z. Ahmad, C. H. Albright, T. Alion, E. Amador, *et al.*, Long-Baseline Neutrino Facility (LBNF) and Deep Underground Neutrino Experiment (DUNE) Conceptual Design Report Volume 1: The LBNF and DUNE Projects (2016), arXiv:1601.05471.

[7] A. Mirizzi, I. Tamborra, H.-T. Janka, N. Saviano, K. Scholberg, R. Bollig, L. Hüdenpohl, and S. Chakraborty, Supernova neutrinos: Production, oscillations and detection, Riv. Nuovo Cim. **39**, 1 (2016).

[8] C. Andreopoulos, A. Bell, D. Bhattacharya, F. Cavanna, J. Dobson, S.Dytman, H. Gallagher, P. Guzowski, R. Hatcher, P. Kehayias, *et al.*, The GENIE Neutrino Monte Carlo Generator, Nucl. Instrum. Meth. **A614**, 87 (2010).

[9] S. Agostinelli, J. Allison, K. Amako, J. Apostolakis, H. Araujo, P. Arce, M. Asai, D. Axen, S. Banerjee, G. Barrand, *et al.*, Geant4-a simulation toolkit, Nucl. Instrum. Meth. A **506**, 250 (2003).

[10] J. Allison, K. Amako, J. Apostolakis, H. Araujo, P. A. Dubois, M. Asai, G. Barrand, R. Capra, S. Chauvie, R. Chytracek, *et al.*, Geant4 developments and applications, IEEE T. Nucl. Sci. **53**, 270 (2006).

[11] J. Allison, K. Amako, J. Apostolakis, P. Arce, M. Asai, T. Aso, E. Bagli, A. Bagulya, S. Banerjee, G. Barrand, *et al.*, Recent developments in Geant4, Nucl. Instrum. Meth. A **835**, 186 (2016).

[12] P. W. Gorham, B. Rotter, P. Allison, O. Banerjee, L. Batten, J. J. Beatty, K. Bechtol, K. Belov, D. Z. Besson, W. R. Binns, *et al.*, Observation of an Unusual Upward-Going Cosmic-Ray-like Event in the Third Flight of ANITA, Phys. Rev. Lett. **121**, 161102 (2018).

[13] J. A. Formaggio and G. P. Zeller, From eV to EeV: Neutrino cross sections across energy scales, Rev. Mod. Phys. **84**, 1307 (2012).

[14] D. A. Krakauer, R. L. Talaga, R. C. Allen, H. H. Chen, R. Hausammann, W. P. Lee, H. J. Mahler, X. Q. Lu, K. C. Wang, T. J. Bowles, *et al.*, Experimental study of neutrino absorption on carbon, Phys. Rev. C **45**, 2450 (1992).

[15] KARMEN Collaboration, Neutrino spectroscopy with KARMEN, Prog. Part. Nucl. Phys. **40**, 183 (1998).

[16] LSND Collaboration, Measurements of charged current reactions of ν_μ on ^{12}C, Phys. Rev. C **66**, 015501 (2002).

[17] J. Meija, T. B. Coplen, M. Berglund, W. A. Brand, P. D. Bièvre, M. Gröning, N. E. Holden, J. Irrgeher, R. D. Loss, T. Walczyk, and T. Prohaska, Isotopic compositions of the elements 2013 (IUPAC Technical Report), Pure Appl. Chem. **88**, 293 (2016).

[18] A. M. Ankowski and J. T. Sobczyk, Argon spectral function and neutrino interactions, Phys. Rev. C **74**, 054316 (2006).

[19] M.-K. Cheoun, E. Ha, and T. Kajino, Reactions on ^{40}Ar involving solar neutrinos and neutrinos from core-collapsing supernovae, Phys. Rev. C **83**, 028801 (2011).

[20] H. Dapo and N. Paar, Neutral-current neutrino-nucleus cross sections based on relativistic nuclear energy density functional, Phys. Rev. C **86**, 035804 (2012).

[21] A. V. Butkevich, Quasi-elastic neutrino charged-current scattering off medium-heavy nuclei: ^{40}Ca and ^{40}Ar, Phys. Rev. C **85**, 065501 (2012).

[22] K. Gallmeister, U. Mosel, and J. Weil, Neutrino-induced reactions on nuclei, Phys. Rev. C **94**, 035502 (2016).

[23] N. Van Dessel, N. Jachowicz, R. González-Jiménez, V. Pandey, and T. Van Cuyck, A dependence of quasielastic charged-current neutrino-nucleus cross sections, Phys. Rev. C **97**, 044616 (2018).

[24] C. Ottermann, C. Schmitt, G. Simon, F. Borkowski, and V. Walther, Elastic electron scattering from ^{40}Ar, Nucl. Phys. A **379**, 396 (1982).

[25] M. Anghinolfi, M. Ripani, R. Cenni, P. Corvisiero, A. Longhi, L. Mazzaschi, V. Mokeev, G. Ricco, M. Taiuti, A. Teglia, *et al.*, Inclusive electron scattering from an oxygen and argon jet target, Journal of Physics G: Nuclear and Particle Physics **21**, L9 (1995).

[26] M. Bhattacharya, A. García, N. I. Kaloskamis, E. G. Adelberger, H. E. Swanson, R. Anne, M. Lewitowicz, M. G. Saint-Laurent, W. Trinder, C. Donzaud, *et al.*, Neutrino absorption efficiency of an ^{40}Ar detector from the β decay of ^{40}Ti, Phys. Rev. C **58**, 3677 (1998).

[27] M. Bhattacharya, C. D. Goodman, and A. García, Weak-interaction strength from charge-exchange reactions versus β decay in the $A = 40$ isoquintet, Phys. Rev. C **80**, 055501 (2009).

[28] K. Langanke, G. Martínez-Pinedo, P. von Neumann-Cosel, and A. Richter, Supernova Inelastic Neutrino-Nucleus Cross Sections from High-Resolution Electron Scattering Experiments and Shell-Model Calculations, Phys. Rev. Lett. **93**, 202501 (2004).

[29] J. Chen, Nuclear Data Sheets for A=40, Nucl. Data Sheets **140**, 1 (2017).

[30] K. Heyde, P. von Neumann-Cosel, and A. Richter, Magnetic Dipole Excitations in Nuclei: Elementary Modes of Nucleonic Motion, Rev. Mod. Phys. **82**, 2365 (2010).

[31] U. Kneissl, N. Pietralla, and A. Zilges, Low-lying dipole modes in vibrational nuclei studied by photon scattering, Journal of Physics G: Nuclear and Particle Physics **32**, R217 (2006).

[32] N. Pietralla, Z. Berant, V. N. Litvinenko, S. Hartman, F. F. Mikhailov, I. V. Pinayev, G. Swift, M. W. Ahmed, J. H. Kelley, S. O. Nelson, *et al.*, Parity measurements of nuclear levels using a free-electron-laser generated γ-ray beam, Phys. Rev. Lett. **88**, 012502 (2001).

[33] U. Kneissl, H. Pitz, and A. Zilges, Investigation of Nuclear Structure by Resonance Fluorescence Scattering, Prog. Part. Nucl. Phys. **37**, 349 (1996).

[34] H. Pai, T. Beck, J. Beller, R. Beyer, M. Bhike, V. Derya, U. Gayer, J. Isaak, Krishichayan, J. Kvasil, *et al.*, Magnetic dipole excitations of ^{50}Cr, Phys. Rev. C **93**, 014318 (2016).

[35] T. C. Li, N. Pietralla, A. P. Tonchev, M. W. Ahmed, T. Ahn, C. Angell, M. A. Blackston, A. Costin, K. J. Keeter, J. Li, *et al.*, First evidence for spin-flip $M1$ strength in ^{40}Ar, Phys. Rev. C **73**, 054306 (2006).

[36] S. Nummela, P. Baumann, E. Caurier, P. Dessagne, A. Jokinen, A. Knipper, G. Le Scornet, C. Miehé, F. Nowacki, M. Oinonen, *et al.*, Spectroscopy of ^{34,35}Si by β decay: $sd-fp$ shell gap and single-particle states, Phys. Rev. C **63**, 044316 (2001).

[37] H. R. Weller, M. W. Ahmed, H. Gao, W. Tornow, Y. K. Wu, M. Gai, and R. Miskimen, Research Opportunities at the Upgraded HIγS Facility, Prog. Part. Nucl. Phys. **62**, 257 (2009).

[38] R. Moreh, W. C. Sellyey, D. C. Sutton, R. Vodhanel, and J. Bar-Touv, Strong photon strength in ^{40}Ar between 8 and 11 mev, Phys. Rev. C **37**, 2418 (1988).

[39] H. Wickert, K. Ackermann, K. Bangert, U. E. P. Berg, C. Bläsing, W. Naatz, A. Ruckelshausen, S. Schennach, and R. Stock, Parities of bound dipole states in ^{40}Ar, Phys. Rev. C **34**, 835 (1986).

[40] K. S. Krane, R. M. Steffen, and R. M. Wheeler, Directional Correlations of Gamma Radiations Emitted from Nuclear States Oriented by Nuclear Reactions or Cryogenic Methods, Atom. Data Nucl. Data **11**, 351 (1973).

[41] H. Junde, H. Su, and Y. Dong, Nuclear Data Sheets for A = 56, Nucl. Data Sheets **112**, 1513 (2011).

[42] A. P. Tonchev, S. L. Hammond, J. H. Kelley, E. Kwan, H. Lenske, G. Rusev, W. Tornow, and N. Tsoneva, Spectral Structure of the Pygmy Dipole Resonance, Phys. Rev. Lett. **104**, 072501 (2010).

[43] P. M. Goddard, N. Cooper, V. Werner, G. Rusev, P. D. Stevenson, A. Rios, C. Bernards, A. Chakraborty, B. P. Crider, J. Glorius, *et al.*, Dipole response of ^{76}Se above 4 MeV, Phys. Rev. C **88**, 064308 (2013).

[44] J. Isaak, D. Savran, M. Krticka, M. Ahmed, J. Beller, E. Fiori, J. Glorius, J. Kelley, B. Löher, N. Pietralla, *et al.*, Constraining Nuclear Photon Strength Functions by the Decay Properties of Photo-excited States, Phys. Lett. B **727**, 361 (2013).

[45] C. Romig, J. Beller, J. Glorius, J. Isaak, J. H. Kelley, E. Kwan, N. Pietralla, V. Yu. Ponomarev, A. Sauerwein, D. Savran, *et al.*, Low-lying Dipole Strength of the Open-Shell Nucleus ^{94}Mo, Phys. Rev. C **88**, 044331 (2013).

[46] D. Savran, T. Aumann, and A. Zilges, Experimental Studies of the Pygmy Dipole Resonance, Prog. Part. Nucl. Phys. **70**, 210 (2013).

[47] M. Scheck, V. Yu. Ponomarev, T. Aumann, J. Beller, M. Fritzsche, J. Isaak, J. H. Kelley, E. Kwan, N. Pietralla, R. Raut, *et al.*, Decay Pattern of the Pygmy Dipole Resonance in ^{60}Ni, Phys. Rev. C **87**, 051304 (2013).

[48] C. T. Angell, R. Hajima, T. Shizuma, B. Ludewigt, and B. J. Quiter, Branching and Fragmentation of Dipole Strength in ^{181}Ta in the Region of the Scissors Mode, Phys. Rev. Lett. **117**, 142501 (2016).

[49] B. Löher, D. Savran, T. Aumann, J. Beller, M. Bhike, N. Cooper, V. Derya, M. Duchêne, J. Endres, A. Hennig, P. Humby, *et al.*, The decay pattern of the Pygmy Dipole Resonance of ^{140}Ce, Phys. Lett. B **756**, 72 (2016).

[50] F. Bečvář, Simulation of γ cascades in complex nuclei with emphasis on assessment of uncertainties of cascade-related quantities, Nucl. Instrum. Meth. A **417**, 434 (1998).

[51] G. F. Knoll, *Radiation Detection and Measurement* (John Wiley & Sons, 1990).

[52] Joint Committee for Guides in Metrology, *Evaluation of measurement data - Guide to the expression of uncertainty in measurement* (JCGM100, 2008).

[53] F. Metzger, Resonance Fluorescence in Nuclei, Prog. Nucl. Phys. **7**, 59 (1959).

[54] D. Savran and J. Isaak, Self-absorption with quasi-monochromatic photon beams, Nucl. Instrum. Meth. A **899**, 28 (2018).

[55] U. Gayer, V. Werner, T. Beck, S. Finch, J. Kleemann, Krishichayan, B. Löher, O. Papst, N. Pietralla, P. C. Ries, *et al.*, Nuclear structure of ^{82}Kr and ^{82}Se relevant for neutrinoless double-beta decay, EPJ Web Conf. **194**, 02004 (2018).

[56] M. Tamkas, E. Açıksöz, J. Isaak, T. Beck, N. Benouaret, M. Bhike, I. Boztosun, A. Durusoy, U. Gayer, Krishichayan, *et al.*, Low-lying dipole strength in the well-deformed nucleus ^{156}Gd, Nucl. Phys. A **987**, 79 (2019).

[57] W. Ritz, Über eine neue Methode zur Lösung gewisser Variationsprobleme der mathematischen Physik., Journal für die reine und angewandte Mathematik (Crelle's Journal) **1909**, 1 (1909).

[58] J. R. Southon, L. K. Fifield, and A. R. Poletti, Lifetimes of excited states in ^{40}Ar, J. Phys. G Nucl. Part. **2**, 117 (1976).

[59] C. W. Foltz, D. I. Sober, L. W. Fagg, H. D. Gräf, A. Richter, E. Spamer, and B. A. Brown, Electroexcitation of low-multipolarity magnetic transitions in ^{36}Ar and ^{38}Ar, Phys. Rev. C **49**, 1359 (1994).

[60] M. Shamsuzzoha Basunia, Nuclear Data Sheets for A = 27, Nuclear Data Sheets **112**, 1875 (2011).

[61] N. Pietralla, T. Li, M. Fritzsche, M. Ahmed, T. Ahn, A. Costin, J. Enders, J. Li, S. Müller, P. von Neumann-Cosel, *et al.*, Competition between excited core states and $1\hbar\omega$ single-particle excitations at comparable energies in ^{207}Pb from photon scattering, Phys. Lett. B **681**, 134 (2009).

[62] J. H. Kelley, J. E. Purcell, and C. G. Sheu, Energy levels of light nuclei a=12, Nucl. Phys. A **968**, 71 (2017).

[63] C. A. Davis, Spin-parity combinations in ^{40}Ar, Phys. Rev. C **20**, 38 (1979).

[64] B. D. Kern, R. W. Winters, and M. E. Jerrell, Beta Decay of ^{40}Cl and Levels of ^{40}Ar, Phys. Rev. C **2**, 948 (1970).

[65] G. Klotz, J. Gonidec, P. Baumann, and G. Walter, Décroissance β de ^{40}Cl, Nucl. Phys. A **197**, 229 (1972).

[66] P. Endt and C. van der Leun, Energy levels of A = 21-44 nuclei (VI), Nucl. Phys. A **310**, 1 (1978).

[67] M. J. Martin, Nuclear Data Sheets for A = 208, Nucl. Data Sheets **108**, 1583 (2007).

[68] B. Özel-Tashenov, J. Enders, H. Lenske, A. M. Krumbholz, E. Litvinova, P. von Neumann-Cosel, I. Poltoratska, A. Richter, G. Rusev, D. Savran, *et al.*, Low-energy dipole strength in ^{112,120}Sn, Phys. Rev. C **90**, 024304 (2014).

[69] A. Krumbholz, P. von Neumann-Cosel, T. Hashimoto, A. Tamii, T. Adachi, C. Bertulani, H. Fujita, Y. Fujita, E. Ganioglu, K. Hatanaka, *et al.*, Low-energy electric dipole response in 120Sn, Physics Letters B **744**, 7 (2015).

[70] G. A. Bartholomew, E. D. Earle, A. J. Ferguson, J. W. Knowles, and M. Lone, Gamma-Ray Strength Functions, Adv. Nucl. Phys. **7**, 229 (1973).

[71] S.-C. Wu, Nuclear Data Sheets for A = 214, Nucl. Data Sheets **110**, 681 (2009).

[72] J. Isaak, D. Savran, B. Löher, T. Beck, M. Bhike, U. Gayer, Krishichayan, N. Pietralla, M. Scheck, W. Tornow, *et al.*, The concept of nuclear photon strength functions: A model-independent approach via $(\vec{\gamma}, \gamma'\gamma'')$ reactions, Phys. Lett. B **788**, 225 (2019).

[73] R. Capote, M. Herman, P. Oblozinsky, P. Young, S. Goriely, T. Belgya, A. Ignatyuk, A. Koning, S. Hilaire, V. Plujko, *et al.*, RIPL − Reference Input Parameter Library for Calculation of Nuclear Reactions and Nuclear Data Evaluations, Nucl. Data Sheets **110**, 3107 (2009).

[74] C. E. Porter and R. G. Thomas, Fluctuations of nuclear reaction widths, Phys. Rev. **104**, 483 (1956).

[75] W. Hauser and H. Feshbach, The Inelastic Scattering of Neutrons, Phys. Rev. **87**, 366 (1952).

[76] T. von Egidy and D. Bucurescu, Systematics of nuclear level density parameters, Phys. Rev. C **72**, 044311 (2005).

[77] S. Goriely and V. Plujko, Simple empirical $E1$ and $M1$ strength functions for practical applications, Phys. Rev. C **99**, 014303 (2019).

[78] A. Voinov, E. Algin, U. Agvaanluvsan, T. Belgya, R. Chankova, M. Guttormsen, G. E. Mitchell, J. Rekstad, A. Schiller, and S. Siem, Large enhancement of radiative strength for soft transitions in the quasicontinuum, Phys. Rev. Lett. **93**, 142504 (2004).

[79] R. Schwengner, S. Frauendorf, and A. C. Larsen, Low-energy enhancement of magnetic dipole radiation, Phys. Rev. Lett. **111**, 232504 (2013).

[80] A. Gilbert and A. G. W. Cameron, A Composite Nuclear Level Density Formula with Shell Corrections, Can. J. Phys. **43**, 1446 (1965).

[81] P. J. Brancazio and A. G. W. Cameron, Relation between Nuclear Level Density Parameters and Mass Shell Corrections, Can. J. Phys. **47**, 1029 (1969).

[82] T. von Egidy and D. Bucurescu, Experimental energy-dependent nuclear spin distributions, Phys. Rev. C **80**, 054310 (2009).

[83] A. Lisetskiy, E. Caurier, K. Langanke, G. Martínez-Pinedo, P. von Neumann-Cosel, F. Nowacki, and A. Richter, Magnetic dipole probes of the sd and pf shell crossing in the ^{36,38}Ar isotopes, Nucl. Phys. A **789**, 114 (2007).